AN ABSTRACT OF THE THESIS OF

JOHN WOLFGANG CZARNIK for the DOCTOR OF PHILOSOPHY
(Name) (Degree)

in PHYSICS presented on 11 August 1971
(Major) (Date)

Title: DISSOCIATIVE EXCITATION OF H_2

Abstract approved: Redacted for privacy
C. E. Fairchild

The form of the velocity distribution of metastable H (2S) atoms produced by dissociative excitation provides evidence of the processes and molecular states involved in the dissociation. In the experiment described here the measured time-of-flight (TOF) distribution--and associated velocity distribution--of H (2S) atoms are interpreted to indicate the predominance of predissociation in the dissociative excitation of H_2 to produce H (2S).

The observation of structure in the TOF distribution of metastable H(2S) atoms produced with kinetic energies less than one electron volt by dissociative excitation is the primary result of the work presented here. The principal difference between the present experimental procedure and previous work is the use of effective cooling of the target molecules through the use of nozzle flow of the H_2 molecules. This effective temperature reduction allows recognition of structure which was not evident in earlier investigations.

The excitation and detection techniques employed are similar to those used previously. Excitation is achieved by a pulsed electron source, a 6AH6 receiving tube with all structure but the cathode and inner two grids removed, operating at a repetition rate of 30kHz. Metastable H(2S) atoms produced by dissociative excitation of H_2 are detected at a distance L from the excitation region by quenching the metastable level and subsequent detection of the Lyman α (1216 A) deexcitation radiation by a Bendix Model 450 channel electron multiplier. Time from excitation to detection is converted to a voltage pulse by an Ortec Model 437A time-to-pulse-height converter (TPHC). The start time of the TPHC is synchronized with the electron gun pulse and the stop signal is the output of the photon detector, the pulse from the light emitted by a metastable. The TPHC OUTPUT is analyzed and displayed by a 400-channel TMC analyzer.

The structure observed in the TOF spectrum of metastable H(2S) atoms is interpreted as evidence of a large extent of predissociation in the dissociative excitation of H_2. Several of the peaks in the TOF distribution are consistently interpretable as due to predissociation of the $D^1\Pi u$ (v=3, 4, 5, 6) excited states of H_2. It is indicated that exceptional broadening of peaks observed in independent spectral studies is caused by predissociation of the $8p\sigma$ (v=4, 5) or $9p\sigma$ (v=5) Rydberg states of H_2. All of the results regarding resolution limit and dependence on the temperature of the target molecules are demonstrated to be consistent with the theory of Stanton and Monahan.

Dissociative Excitation of H_2

by

John Wolfgang Czarnik

A THESIS

submitted to

Oregon State University

in partial fulfillment of
the requirements for the
degree of

Doctor of Philosophy

June 1972

APPROVED:

Redacted for privacy

Associate Professor of Physics
in charge of major

Redacted for privacy

Chairman of Department of Physics

Redacted for privacy

Dean of Graduate School

Date thesis is presented August 11, 1971

Typed by Muriel Davis for John Wolfgang Czarnik

ACKNOWLEDGMENT

The author is grateful for the consistent encouragement, assistance, and constructive criticism from Dr. Clifford Fairchild. Discussions with several faculty members and graduate students at Oregon State University have contributed to this work and are gratefully acknowledged. In a different, but very important way, the understanding and encouragement of the author's wife, Mary, has significantly contributed to the performance and presentation of the work described in this thesis.

TABLE OF CONTENTS

LIST OF FIGURES

DISSOCIATIVE EXCITATION OF H_2

INTRODUCTION

The velocity distribution of metastable H(2S) atoms produced by electron bombardment of H_2 molecules is an important physical quantity in certain atomic beam experiments, atmospheric observations, and in the determination of the molecular states and processes involved in the production of the metastables. Measurements of the Lamb shift in atomic hydrogen are affected by the velocity distribution of H(2S) atoms used in the experiment (26). Temperatures which are inferred from Doppler broadening of Lyman α (1216Å) in the atmospheric nightglow (1, 8, 42) can be in error if a portion of the observed radiation originates from H(2S) atoms which have sufficiently high velocity. Leventhal, et al. (27) have interpreted observed metastable velocity distributions to signify the existence of a Franck-Condon "forbidden" transition to certain states of H_2 in the excitation process.

The principal result of the work presented here is a new measurement of the velocity distribution of H(2S) atoms produced by electron bombardment of H_2. The new data indicate that predissociation of particular bound states of H_2 is the predominant mechanism for the production of these metastables. This interpretation is in

contrast to previous indications (10, 11, 27) that direct dissociation accounts for the production of metastables in dissociative excitation of H_2. The distinctive feature of this experiment, reduction of the temperature of the target molecules, is discussed in Chapter 3.

The two mechanisms for dissociative excitation, direct dissociation and predissociation, can be explained with the use of the molecular potential energy curves presented in Figures 1 and 2.

Direct dissociation by excitation to a state characterized by a potential energy curve with no bound states is indicated by the arrow labelled 1 in Figure 1. Direct dissociation by excitation to an unbound state associated with a molecular potential curves which does possess bound states is indicated by the arrow labelled 2. Atoms produced in each case share an amount of kinetic energy represented by the distance between the respective total energy lines (dashed) and the potential energy curves as the internuclear separation R approaches infinity, roughly that energy indicated toward the right side of Figure 1. The entire process occurs in a time comparable to the period of a molecular vibration. For the excited states of H_2 this time is approximately 10^{-14} seconds.

Predissociation refers to an excitation to a bound state which then decays via a radiationless transition to an unbound state of the molecule. An example of this process is depicted in Figure 2 by the excitation labelled 1, to the bound $D^1\Pi_u$ state, then a transition

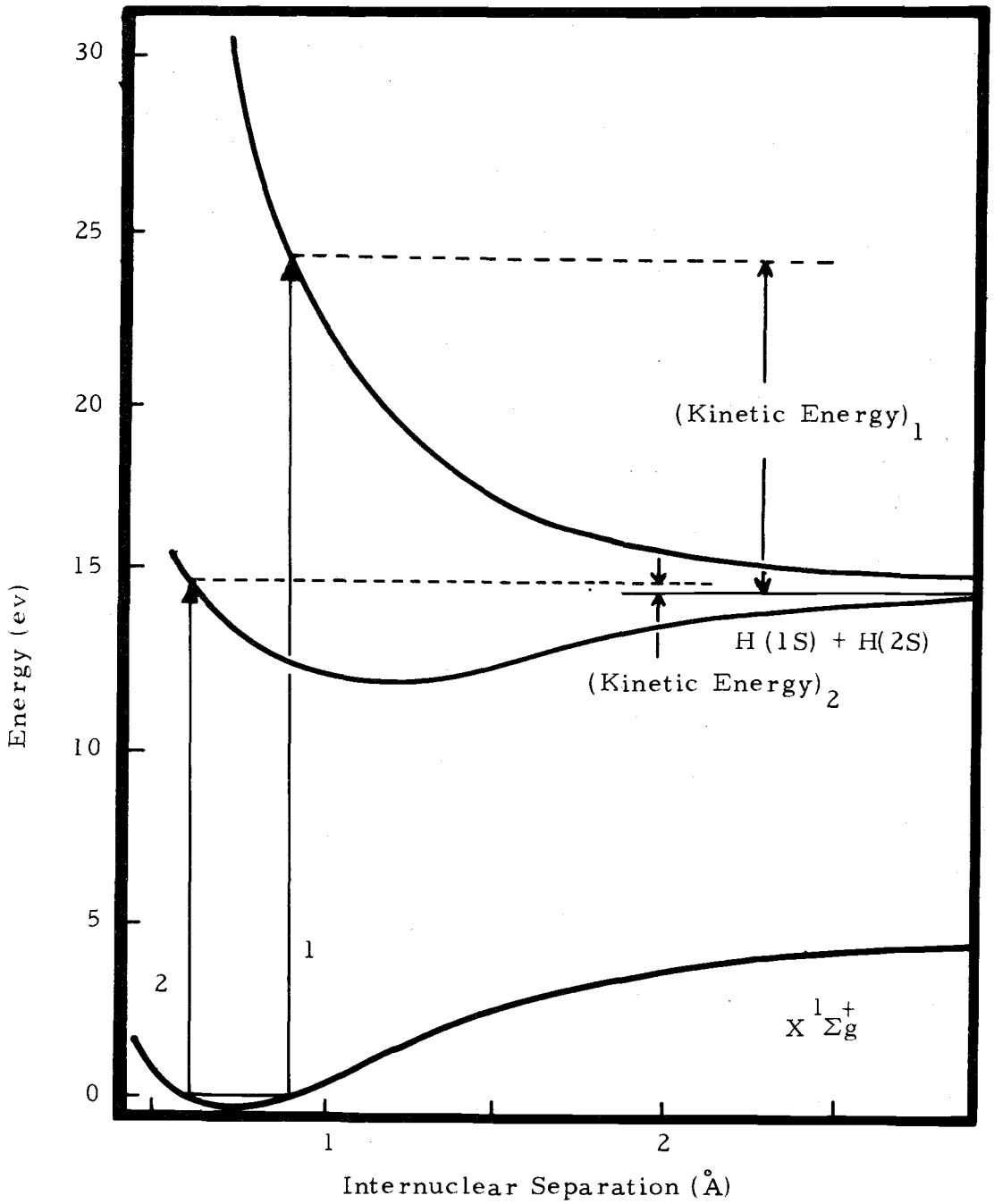

Figure 1. Dissociative excitation to unbound states of H_2. Direct dissociation is demonstrated by transition 2 to an unbound state associated with a molecular potential curve with bound states and by transition 1 to a state on a curve which has no bound states. The horizontal dashed lines indicate the total energy of the excited states. The kinetic energy at infinite separation is indicated for each state.

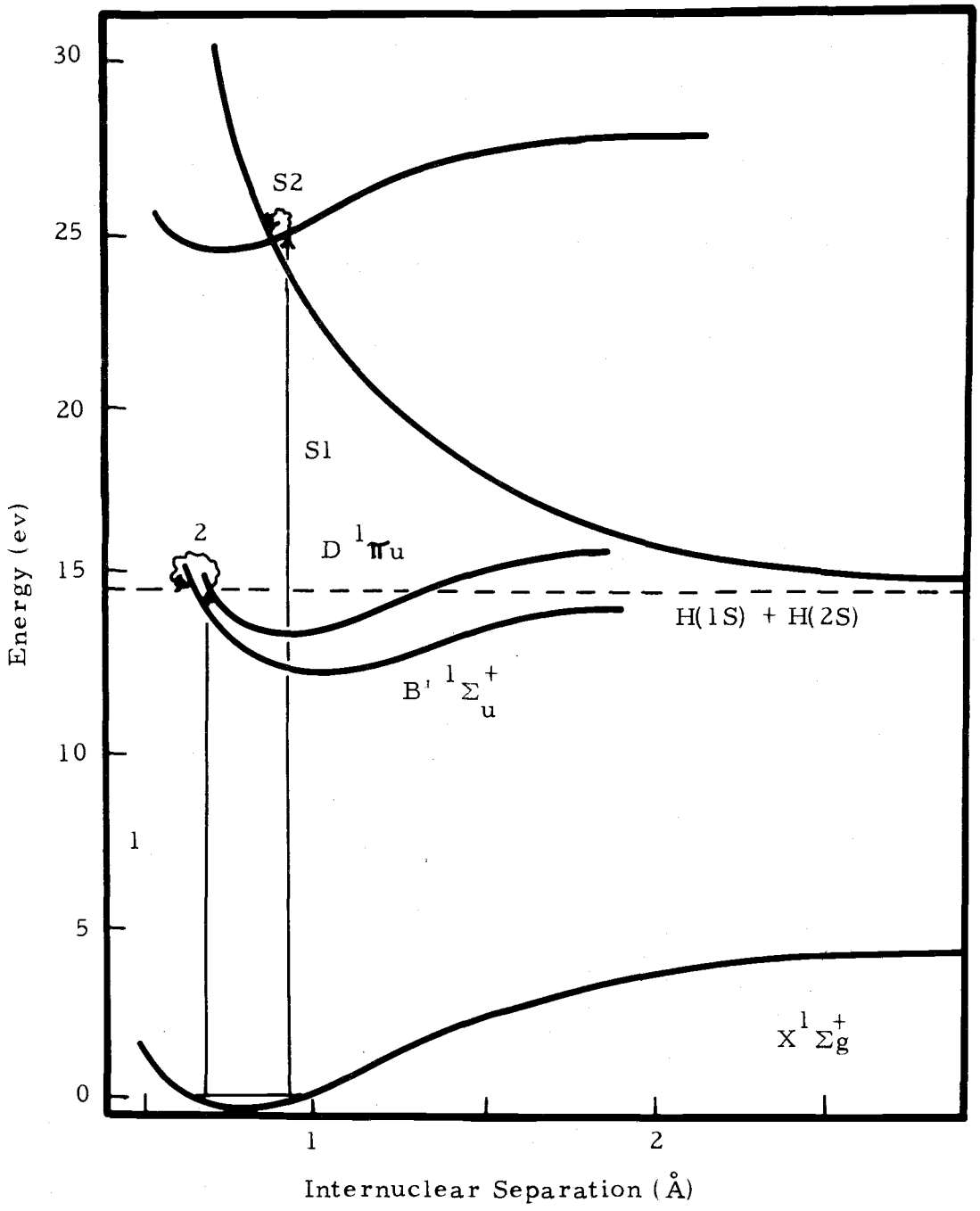

Figure 2. Predissociation in dissociative excitation. S1 and 1 are transitions to bound states. Transitions S2 and 2 occur via mixing, or "crossing", with the nearby unbound states. The kinetic energy of the dissociation products is similar to that shown in Figure 1.

(curved line labelled 2) to an unbound state in the continuum of the $B' {}^1\Sigma_u^+$ level. Transitions S1 and S2 demonstrate predissociation to a state characterized by a repulsive potential curve.

Within the framework of the Born-Oppenheimer approximation which is discussed in more detail in Chapter 4, the effective static potential for the electrons is calculated as a harmonic series for a fixed internuclear separation, R. The series expansion for the potential is terminated at some appropriate term, then this truncated series is used to calculate the energy eigenvalues for the electronic wave functions. The perturbations which produce dissociation within this set of basis states by coupling the electronic states are the terms in the exact Hamiltonian which describe the nuclear motion. These are neglected in calculating the electronic wave function and energy eigenvalues in the spirit of the approximation of the potential at a fixed R.

The types of predissociation are classified according to the character of the excited states which couple to produce the dissociation. The two types of predissociation which can occur in H_2 are labelled I and III by Herzberg (19, p. 413). Case I predissocation occurs because of the overlapping of the bound electronic state by the dissociation continuum belonging to another electronic state. This is the case described in Figure 2 and the most important case in the interpretation of the experimental results reported here. In

case III, predissociation takes place because of the overlapping of the high rotational levels of a given electronic state with the dissociation limit of the same electronic state. Several predissociation rates have been calculated and are of the order of 10^6 to 10^{13} per second.

The processes and states involved in the dissociation of H_2 into H(2S) and another product atom can be inferred from a knowledge of the velocity distribution of H(2S) atoms and the excitation conditions. For example, a broad continuous distribution of velocities, and corresponding energies, would be expected in excitation 1 of Figure 1. The final vibrational states for a given spread of excitation energies have a continuous range of kinetic energies of the product atoms. In contrast, the excitation S1 of Figure 2 has discrete vibrational levels as the exicted states. The relatively narrow width of these levels can produce separate peaks in the energy and velocity distribution of the final predissociated atoms if the excitation energy allows for production of these excited states and thermal effects do not broaden such structure beyond recognition. The thermal effects and the relationship between an observed velocity distribution of H(2S) atoms and molecular processes for H_2 is developed in the following chapter. However, at this point in the discussion it is convenient to introduce the experimental method used to obtain a velocity distribution.

The H(2S) velocity and energy are

$$V = L/t \tag{1.1}$$

$$E = m(L/t)^2/2 \tag{1.2}$$

where m is the mass of a hydrogen atom. The energy distribution, $P(E)$, can be determined from the time-of-flight distribution, $P(t)$, by the transformation

$$P(E) = P(t) \cdot dE/dt \, . \tag{1.3}$$

Assuming that the two hydrogen atoms produced in the dissociation have equal kinetic energies, E, the energy of the molecular state from which they were produced is calculated as E_e,

$$E_e = 2E + E_d + E_{2S} \tag{1.4}$$

where E_d is the threshold energy for dissociation of H_2 and E_{2S} is the energy difference between the $2S$ and $1S$ states of atomic hydrogen.

Although atoms in many excited states are produced during excitation, only metastable $H(2S)$ atoms are detected directly. Atoms in other excited states decay radiatively before they move far from the point of excitation. Ground state atoms produce no response from the detection system.

TEMPERATURE DEPENDENCE OF TIME-OF-FLIGHT DISTRIBUTION

The target H_2 molecules involved in the dissociative excitation are in the gas phase; thus, the velocity distribution of the atomic products is affected by the random thermal motion of these target molecules. A simple example will illustrate this effect. If all metastable atoms are produced with a single value of kinetic energy, E_o, from molecules at rest, they will all travel a distance L to a detector in a time

$$t_o = L \sqrt{\frac{m}{2E_o}} \qquad (2.1)$$

where m is the mass of a metastable atom. If the parent molecules are in motion with a single kinetic energy E_M, some of them will have velocities directed toward the detector at the time of dissociation and some will have velocities directed away from the detector. The times of arrival of metastables in these two extreme cases will be

$$t_{\pm} = \frac{L}{\sqrt{\frac{2E_o}{m}} \pm \sqrt{\frac{2E_M}{M}}} \qquad (2.2)$$

in which M is the mass of the hydrogen molecule. In this simple example a distribution of times of arrival at the detector for metastables produced with a single energy in the rest frame of

monoenergetic molecules reflects the thermal motion of the parent molecules.

In general the molecular velocities will have a distribution in both magnitude and direction. In the following discussion the distribution of dissociation products is assumed to be isotropic in the center of mass frame. If an amount of energy, Q, is converted to kinetic energy of the atoms, then for each E_M the distribution of kinetic energy, E, of the atoms is (39)

$$\mathcal{P}_{E_M,\,Q}(E) = \begin{cases} \dfrac{1}{2(QE_M)^{1/2}} & \text{for } E_- < E < E_+ \\ 0 & \text{otherwise} \end{cases} \qquad (2.3)$$

$$E_\pm = \frac{1}{2}\left(E_M^{1/2} \pm Q^{1/2}\right)^2 , \qquad (2.4)$$

A derivation of this energy distribution and the accompanying limits is presented in Appendix A. If the parent molecules have a Maxwellian velocity distribution, the resulting distribution of energies of the atoms produced by dissociation will be

$$P(E) = \int_o^\infty dQ \int_o^\infty dE_M \; \frac{F(Q)}{Q^{1/2}\pi^{1/2}\theta^{3/2}} \; e^{-E_M/\theta} \qquad (2.5)$$

where $\theta = kT$, k is the Boltzmann constant, and T is the absolute temperature of the target H_2 molecules. F(Q) is the distribution of

the energy Q which depends on the form of the potential energy curves of the molecule. If the dissociation process occurs from a continuum of dissociating states, as happens in the excitation labelled 1 of Figure 1, the distribution F(Q) is non-zero over a wider range of values of Q than if predissociation from a discrete vibrational state is producing the dissociated atoms. This occurs because for a "steep" excited state potential curve the range of values of final state energies over which the excitation matrix elements contribute, for a fixed range of internuclear separation (near the classical turning points of the ground state potential curve) is larger than for a "shallow" curve. If the dissociation is assumed to be from a discrete energy level, i.e., predissociation, F(Q) can be expressed as a delta function, $\delta(Q-2E_o)$ where $2E_o$ is the kinetic energy available to the two dissociating atoms. Equation (2.5) can be integrated to produce an explicit expression for the energy distribution of the atoms produced in predissociation. The result is

$$P(E) = \frac{2^{1/2}}{(\pi\theta E)^{1/2}} e^{-2\frac{(E+E_o)}{\theta}} \sinh\left(4\sqrt{\frac{EE_o}{\theta}}\right) \qquad (2.6)$$

This delta function approximation is applicable to the predissociation process because the range of energies of the dissociating atoms is small compared to the excitation energy and the kinetic energy of the dissociating atoms. The range of energies available to the dissociating atoms is roughly 0.003 ev, which corresponds to the 1Å

predissociation rate of 10^{12} sec^{-1} as calculated by Nielsen and Berry (34). At 700 Å the excitation energy is 17.6 ev. Excitation to states associated with a directly dissociating molecular potential curve may produce an energy range of one electron volt or more (18) for the dissociating H(2S) atoms, depending upon the particular final states involved in the dissociation process.

Equations (1.2) and (1.3) serve to convert the energy distribution of (2.6) into a time-of-flight distribution. For the states of interest in this experiment the excess energy above dissociation, E_o, is greater than 0.25 ev. The cooling effect described in Appendix B reduces the effective temperature of the target gas so that θ is approximately 0.004 ev. Thus, the term in Equation (2.6) which contains the negative exponential part of the sinh function is negligible and the approximate time-of-flight distribution is

$$P(t) \propto \frac{1}{t^3} e^{-A\left(\frac{1}{t} - \frac{1}{t_o}\right)^2} \qquad (2.7)$$

where t_o is the time-of-flight that would be observed if the parent molecules were at rest at the time of dissociation. The temperature dependent quantity A is equal to ML^2/θ.

By forming linear combinations of the functions described in Equation (2.7) with different values of t_o, it was determined that an effective H_2 temperature of approximately 60° K is required to resolve the structure due to predissociation in two or more adjacent

vibrational levels of H_2 in the time-of-flight spectrum. The random momentum gained by the molecules during electron excitation corresponds to about 50° K. Thus the structure due to predissociation can be seen only if the target molecules are at a sufficiently low temperature before excitation. The development of Equation (2.6) for the case in which $F(Q)$ is not a delta function (as would be the case for the excitation shown in Figure 1) is not described here because the results of the present experiments are consistent with the interpretation that the process $e + H_2 \rightarrow e' + H + H(2S)$, in which the prime denotes inelastic scattering, proceeds almost exclusively by predissociation.

EXPERIMENTAL TECHNIQUE AND APPARATUS

As indicated previously, the velocity distribution of metastable H(2S) atoms produced by dissociative excitation of H_2 is determined by measuring the time-of-flight of the metastables. The time-of-flight spectrum is obtained by bombarding an H_2 gas target with a short burst of electrons at time $t = 0$ and detecting the H(2S) atoms at a later time t at a distance L from the point of production. In practice, since the excitation and detection regions are finite, L is only approximately the same for all atoms. The atoms are detected by quenching them in a dc electric field and observing the resultant Lyman α radiation with a photomultiplier. In the presence of a weak electric field the 2S levels of H lose their metastability because of mixing with the 2P levels (5, p. 370; 25). A time-of-flight spectrum is accumulated by exciting the target gas repeatedly at regular intervals and storing each Lyman α pulse (with its time signature) which is detected by the photomultiplier. With the electron gun pulsed at a repetition rate of 30 kHz the H(2S) count rate is typically one count per second. The kinetic energy of the projectile electrons was 25 electron volts or greater in all final data runs in order to achieve this count rate. A photomultiplier with a bare cathode is used as the detector so that the efficiency for the detection of Lyman α emitted by metastable H(2S) atoms is maximized. Photons are

detected from fast and slow H(2S) atoms which emit within view of the photomultiplier. Both the intended quenching field which is discussed in this chapter and quenching by collision at surfaces can produce photons from the H(2S) atoms.

With 25 electron volts of excitation energy there are several processes occurring which might conceivably contribute "background" to the H(2S) signal:

1. molecular radiative decay:

$$e + H_2 \rightarrow e + H_2^*$$

$$H_2^* \rightarrow H_2 + \text{photon}$$

$$H_2^* (\text{collision with wall}) \rightarrow H_2 + \text{photon}$$

2. ionization

$$e + H_2 \rightarrow 2e + H_2^+$$

3. dissociative ionization

$$e + H_2 \rightarrow H + H^+ + e + e'$$

4. dissociative attachment

$$e + H_2 \rightarrow H + H^-$$

5. Auger processes

$$H_2^* + \text{surface} \rightarrow H_2 + \text{electron}$$

$$H(2S) + \text{surface} \rightarrow H(1S) + \text{electron}$$

In the above expressions the asterisk denotes an excited state of the molecule. Since the detector used in this experiment has a bare cathode, care must be taken to avoid or minimize detection of the ions, electrons, and ultraviolet photons produced by these processes. Electrons scattered from the excitation region and those produced by the Auger processes can produce a very large background, so a magnetic field and a negative detector bias are adjusted to minimize this contribution to the background. This technique does not discriminate against the H^- ions as well as the electrons since the ions can be produced and accelerated in the excitation region during the excitation pulse. The larger mass of H^- ions and their range of kinetic energies does not allow simultaneous optimum reduction of the contributions from both Auger electrons and H^- ions by the methods employed to minimize the electron signal. Photons from H(2P) states created during the excitation process might also be detected during and immediately after excitation. If all of these processes were detected, the accumulated time-of-flight spectrum might appear somewhat like Figure 3.

The photon peak ($h\nu$) near $t=0$ is due to excitation and radiative decay. This signal is avoided by placing the detector so that it does not directly view the excitation region. In the figure the location of the signals due to the ions is somewhat arbitrary since small stray electric fields can influence their velocity. A retarding electric field

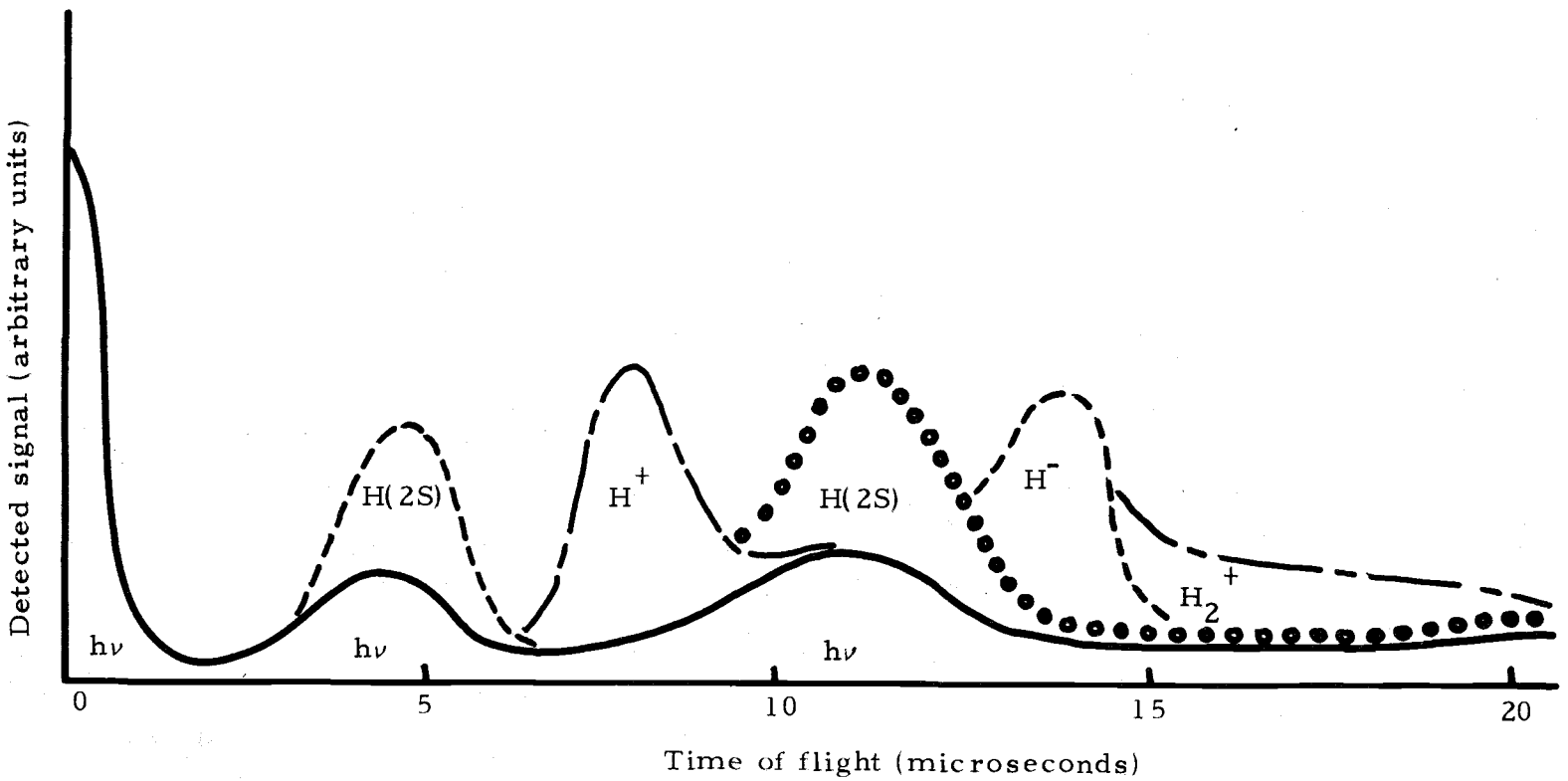

Figure 3. Hypothetical time-of-flight spectrum. If H^-, H^+, H_2^+, and all the Lyman ($h\nu$) from the metastables were all detected, the spectrum might appear as depicted. The solid line is the contribution of photons. The ultraviolet contribution near t=0 may contain some scattered radiation from the excitation region. The two $h\nu$ peaks near 4 and 11 microseconds are due to metastables quenched in the electric field. The "H(2S)" enveloping these peaks are meant to signify metastables detected by collision with the detection cathode, or after quenching at other surfaces.

cannot be used to deflect the ions before reaching the detector since such a field would, as discussed later in this chapter, quench the H(2S) atoms before they arrive at the detector region. Neither can magnetic fields be used to effectively deflect the ions from the detector region because these ions can be reflected upon incidence at wall surfaces. The photon peaks shown at 3.5 and 10 microseconds are due to the H(2S) atoms which are perturbed in front of the detector and then radiate. The associated overlying peak labelled "H(2S)" can be due to metastables which actually strike the detector surface. The separation of the photon signal due to the arriving H(2S) atoms from the background due to ions is achieved by accumulating time-of-flight spectra with and without application of a radiofrequency (rf) field which causes the metastables to radiate at a position along their flight path where the resulting 1216 Å radiation cannot be detected. As will be shown later in this chapter, this rf field cannot affect the ions passing through the rf region. The signal due to the metastable H(2S) is obtained by subtracting the signal produced when the rf field is applied from the time-of-flight spectrum produced when the rf field is not present.

The experimental apparatus, shown schematically in Figure 4, was designed to provide the following characteristics:

a. low base pressure and cleanliness in order to avoid contamination of the hydrogen gas and maintain a low enough

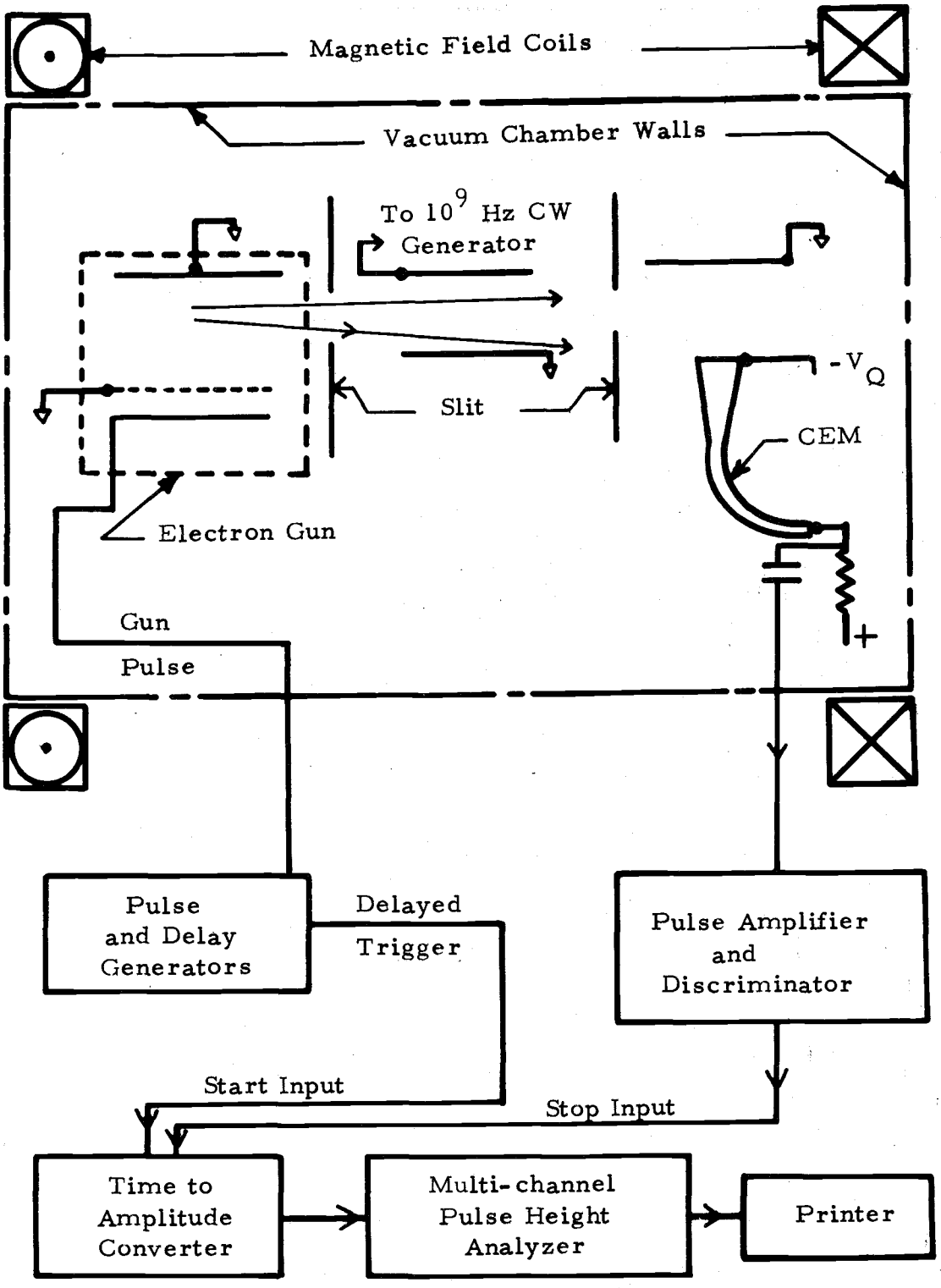

Figure 4. Schematic diagram of experimental apparatus.

operating pressure so that pressure quenching of the metastable H(2S) atoms would be minimal.

b. cooling of the target gas molecules so that any structure in the time-of-flight spectrum of metastable atoms could be readily detected.

c. an intense source of electrons which can be pulsed repeatedly with a pulse width less than 0.1 microsecond and at repetition rates of about 30 kHz.

d. a small dc electric field quench region to quench all metastables that enter this region.

e. a means to separate the signal due to meastables from background counts due to charged particles and extraneous photons.

f. collimation and confinement of the electrons in the excitation region.

g. adequate stability and resolution in the timing electronics so that the time-of-flight distribution could be determined within an absolute error of ± 0.5 microseconds; this resolution is necessary for interpretation of the observed structure.

The following sections contain a detailed description of the components of the experimental equipment and their functions.

Excitation Chamber and Vacuum System

An operating pressure of less than 5×10^{-4} torr is required to avoid quenching the H(2S) atoms by collisions with molecules. A mean free path of a metastable at this pressure, 20 centimeters, or approximately twice the time-of-flight path used here, is calculated from the collisional quenching cross section obtained by Fite and Brackman (17). More recent measurements indicate that at the operating pressure used here, less than 20 percent of the metastable H(2S) atoms produced are quenched by collision with molecules during their motion from between the excitation region and the detector (29).

The excitation chamber, shown in Figure 5, consists of a four liter stainless steel cylinder, seven centimeters in radius, with a cylindrical table, five centimeters in radius, placed in the center and sealed to the bottom of the large chamber. The table top has a 0.2×0.9 centimeter slit over which a 1.0 centimeter I.D. stainless steel tube, ten centimeters long, is mounted. An identical slit, above which the electron gun is mounted, was cut in the stainless steel covering plate at the top end of this tube. A second larger hole in the table top is fitted with a tube that seals to the cover of the outer chamber so that a Varian ionization gauge, range $10^{-4} - 10^{-11}$ torr, mounted in the cover, can monitor the pressure in the region under

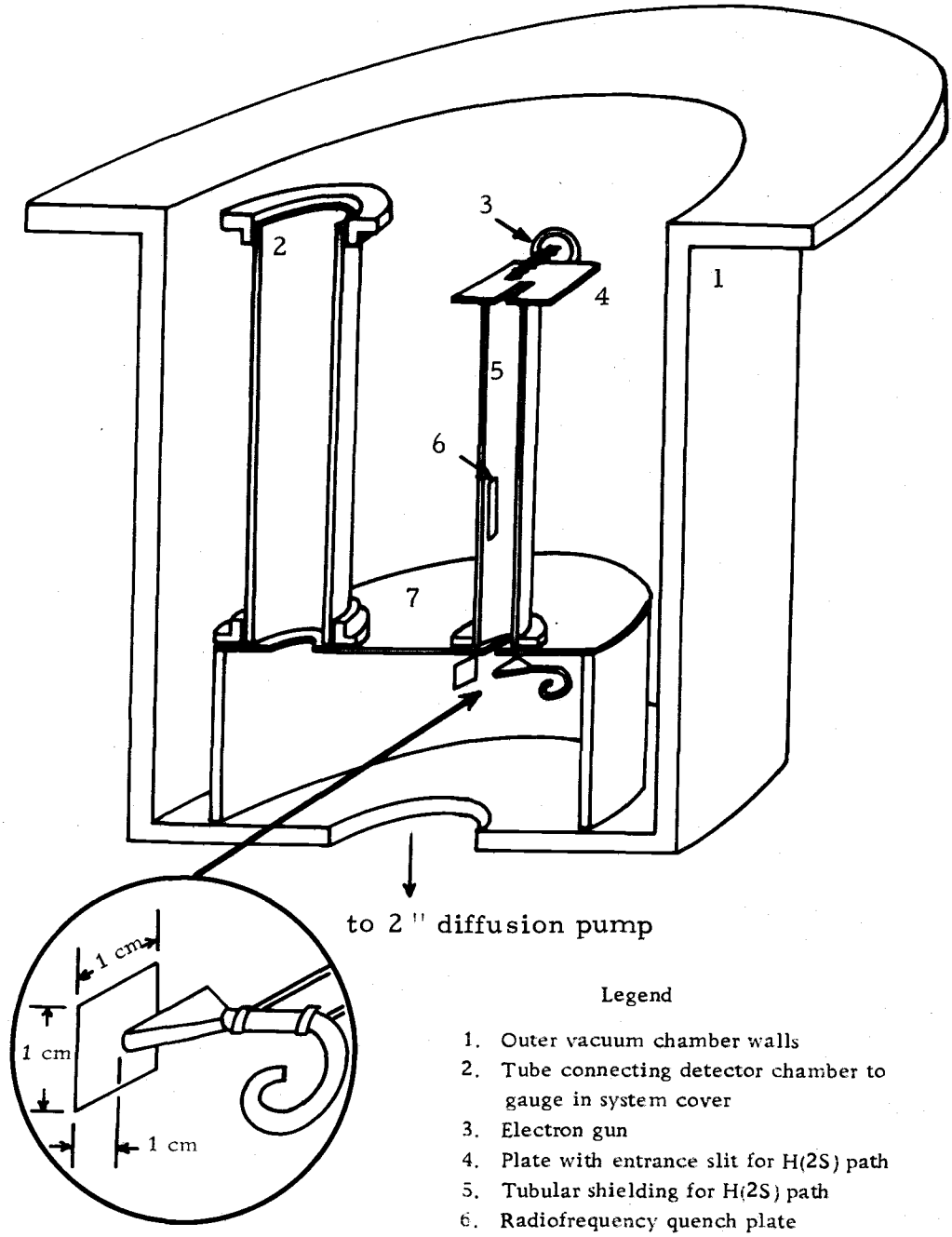

Detail A

Legend

1. Outer vacuum chamber walls
2. Tube connecting detector chamber to gauge in system cover
3. Electron gun
4. Plate with entrance slit for H(2S) path
5. Tubular shielding for H(2S) path
6. Radiofrequency quench plate
7. Top of detector chamber
8. Electron multiplier
9. Grounded plate
10. Glass mounting hooks for electron multiplier

Figure 5. Cross-sectional view of excitation and detection chambers.

the inner table, hereafter called the detector chamber.

Another pressure gauge, a Varian Milli-Torr ionization gauge, range 10^{-1} - 10^{-7} torr, is located in the cover and exposed to the main chamber in which the excitation occurs. During the experiment this gauge is turned off to prevent ultraviolet radiation from entering the excitation region. A Vac-Ion pump (trademark Varian Corporation) provides pumping and secondary pressure measurement in an auxiliary side chamber which is connected to the main chamber by a one inch circular hole.

The region below the detector chamber contains a Sorbent A (trademark Consolidated Vacuum Corporation) pellet trap which leads through a baffle to a two-inch diffusion pump backed by a liquid nitrogen trap and a forepump. During pumpdown the pellets are baked at a pressure of approximately 10^{-2} torr to drive off adsorbed water vapor. While the diffusion pump is being started, a gate valve located between the pellet trap and the diffusion pump is closed. During operation the pellets adsorb pump oil and inhibit its entry into the detector and excitation chambers. The entire system maintains a base pressure of less than 5×10^{-7} torr.

Handling and Cooling of the Target Gas

Matheson research grade hydrogen gas is delivered to the excitation region through a Matheson Model 18 Transfer Regulator,

30 centimeters of 0.25 inch I.D. stainless steel tubing, and a Vacoa Corporation MV-25 stainless steel gas metering valve. Although the temperature of the gas on the low pressure side of the valve is not measured, the time-of-flight data can be consistently interpreted by assuming that the target molecules are reduced to a temperature of less than 60° K by expansion in the needle valve. Typically the gas pressure at the low pressure side of the needle valve is 10^{-7} atmospheres. (The latter pressure is obtained by measuring the pressure in the excitation region and estimating both the pumping speed of the system and the flow impedance between the excitation region and the needle valve.)

In order for a temperature reduction to occur, the heat transfer to the expanding gas from the needle valve, which is at room temperature, must be small. In most supersonic flows of compressible gases, the effects of interaction with the walls are experienced by a thin layer near the walls confining the flow (28, p. 233). In addition, the coefficient of accommodation (the fraction of energy exchanged in the collision between a wall and a molecule from a gas which is not at the equilibrium temperature of the wall) may be very small for H_2 on stainless steel. Although accommodation coefficients of many gases on metal surfaces have measured (38, 40), that of H_2 on stainless steel has not been studied to the best of this writer's knowledge. Previous calculations and experiments (2, 3, 23) have indicated that

heat transfer to the main flow of gas from the walls must be relatively insignificant for flow of a compressible gas through a convergent-divergent valve (a Laval nozzle).

Under the adiabatic nonviscous streamline conditions proposed above, the flow of a compressible fluid can be described by the equation (20, p. 101)

$$p\rho^{-5/3} = \text{Constant} \qquad (3.1)$$

where p is the gas pressure at a point and ρ is the mass density at the same point. This equation is the same in form as that for the reversible adiabatic (isentropic) expansion of an ideal diatomic gas. The gas cools as it does work on the surrounding gas and increases the mass flow energy (which is demonstrated in Appendix B). The H_2 temperature and pressure after the expansion, T and p are related to the corresponding quantities, T_o and p_o before the expansion, by the relation

$$\frac{T}{T_o} = \left(\frac{p}{p_o}\right)^{+2/5} \qquad (3.2)$$

This mechanism provides adequate temperature reduction for the target gas, as was discussed in Chapter 2.

Electron Gun

The electron gun consists of the cathode, control grid, and screen grid of a 6AH6 receiving tube. Small capacitance and relatively

small spacing provide this structure with sharp rise- and fall-time characteristics. Also, the small volume of the gun, 1 mm x 2 mm x 15 mm serves to help satisfy the requirement that the excitation take place at a point, or, with the geometry described on pages 20-22, along a line. The glass envelope of the tube is cut close to the base and the upper portion of the envelope is removed. After the outer structure of the tube has been removed this electron gun is soldered to the heater, cathode, and grid lead wires which lead to the vacuum feed-throughs. The gun is then positioned above the slit in the narrow tube leading to the detector chamber, as shown in Figure 5.

The cathode heater on the electron gun is maintained at 1.5 volts during the pumpdown to 10^{-6} torr to keep water vapor off the structure without overheating the cathode coating. The heater voltage is then increased slowly to the operating voltage of nominally 8.0 volts. The normal operating voltage of this tube, 6.5 volts, is exceeded in order to increase the emission current. Both a Lambda regulated dc power supply and a Variac with a filament transformer were used as heater voltage sources in order to ensure that the magnetic field caused by dc in the heater wire was not affecting the path of electrons in the excitation region. The change of power supplies without a resulting alteration of the time-of-flight distribution also confirms that electric fields produced by the various parts of the tube structure do not significantly affect the excitation or quenching

H(2S) in the region of electron bombardment.

Both grids of the tube are grounded. Electrons in the space charge surrounding the cathode are accelerated by a negative voltage pulse applied to the cathode. This pulse is provided by a E-H Model 120D pulse generator terminated in 50 ohms. Previous experiments performed in this laboratory have demonstrated that a falltime of less than 4 nanoseconds is characteristic of the electron pulse produced by this type of gun and pulser arrangement (31, p. 22).

Detector and Detector Quench Region

The hydrogen atoms in the 2S state which are produced in the excitation region travel a distance of ten centimeters and enter a region of constant electric field in front of the detector. The radiative lifetime of an unperturbed metastable hydrogen atom is one-seventh of a second. In a moderate electric field, the lifetime of the 2S, τ_s, is (5, p. 370; 25).

$$\tau_s = \{\hbar^2(\omega^2 + \gamma^2)/V^2\} \cdot 1.6 \cdot 10^{-9} \text{ seconds} \qquad (3.3)$$

where V is the matrix element $(2P \mid eE \cdot r \mid 2S)$ between the 2S and 2P state of hydrogen, $h\omega$ is the energy splitting between these states, and $\hbar\gamma$ is the energy width of the 2P state. This expression indicates that a field of 100 volts/cm should reduce the lifetime of the metastable to less than 0.05 microsecond.

In the present experiment, a static electric quench field of approximately 200 volts/cm is produced by the negative voltage bias on the cathode of a Bendix Model 450 channel electron multiplier (CEM). The cathode of the CEM is the portion of the CEM furthest to the left in Figure 5 and in Detail A of Figure 5. The positioning of the slit, detector, and one-inch square stainless steel plate (at electric ground potential) opposite the detector was chosen (by a water bath potential determination and by approximate calculation) to minimize fringing fields so that the metastables would not be quenched before reaching the region in front of the detector. The CEM was used as the detector in this experiment because of its narrow pulse height distribution (refer to Figure 6), its efficiency for detection of Lyman α, and its relatively large current output pulses of 10^{-11} coulombs (20 to 100 millivolts delivered into a 50 ohm termination).

The cathode of the CEM, as depicted in Detail A of Figure 5, is shaped like a squashed cone with outer dimensions 0.2 x 0.8 cm. The outer edge of the cathode is biased at -40 volts. The narrow end of the cathode, which is attached to the spiral-shaped continuous dynode tube is grounded and the opposite end of the dynode is maintained at nominally +3500 volts. A Lyman α (1216 Å) photon emitted by a quenched metastable in a 0.5 cm^3 volume in front of the cathode impinges on the inner cathode surface and causes ejection of en electron which is multiplied as it is accelerated toward the positive

end of the dynode structure. The dynode "tube" is 5 centimeters long and has an inner diameter of 0.15 centimeters. If it is assumed that an electron starting with zero velocity at the cathode end of the dynode strip travels 0.2 centimeters between striking the surface of the dynode, then it is accelerated again from zero velocity in subsequent 0.2 centimeter segments, the delay time between the ejection of the electron from the cathode to the output at the anode of CEM is at most 0.065 microseconds. This delay is smaller than the uncertainty in the setting of the delayed trigger (see Figure 4) which starts the time-to-pulse-height converter.

The largest error in determining the time-of-flight occurs because of the uncertainties in the location of the points of creation and detection of the metastables. This error is estimated to be ±0.5 centimeters along the 10.8 centimeter path from the electron gun to the detector.

Radiofrequency Quench Region

As mentioned in the beginning of this chapter, a radiofrequency (rf) quench region is placed midway between the electron gun and the detector, along the path of the metastables (refer to Figures 4 and 5) in order to separate the signal due to ions from the signal due to the H(2S) atoms. The rf electric field oscillates between ±20 volts at a frequency of about 1.06×10^9 Hertz (the Lamb shift frequency),

so that the ions which are moving through this region are not deflected. The response of the ions to such a rapidly oscillating field is negligible because before much momentum has been imparted to an ion by a positive (or negative) portion of a cycle, the other portion decelerates the ion. The time-of-travel of the ions through the quench region, of the order of one microsecond, is very long compared to the period at oscillation of the rf field so that the ions are not deflected by the field.

When the 1060 MHz rf signal from a Radio Research Laboratory (Harvard University) F3500 Airborne Radar Jammer (AN/APT-5) is applied to this region, metastable H(2S) atoms are quenched: they emit Lyman α radiation.

The lifetime for decay of H(2S) to H(2P) in an rf field of energy density S_o and frequency ω, is approximately (26)

$$\tau_s = \frac{hc^2}{2\pi e^2 \gamma S_o} \quad \frac{[(\omega - \omega_o)^2 + (\gamma/2)^2]}{|(2P|\hat{e}\cdot\vec{r}|2S)|^2} \qquad (3.4)$$

in which $\hbar\omega_o$ is the energy difference between H(2S) and H(2P), $\gamma = 1/\tau_p$ is the radiative damping constant of the 2P state. The matrix element, $(2P|\hat{e}\cdot\vec{r}|2S)$ (in which $\hat{e}$ is the direction of the electron polarization vector of the field) is one of the order of a_o, where a_o is the classical Bohr radius, 5.3×10^{-9} centimeters. Thus, the lifetime of a metastable H(2S) atom in an rf field at the resonant frequency $\omega_o = 1060$ MHz is

$$\tau_s = \frac{\gamma \hbar c^2}{8\pi e^2 a_o^2 S_o} \qquad (3.5)$$

The fraction of H(2S) atoms with a velocity v that are quenched in an rf field that is ℓ centimeters long is (25)

$$\text{fraction quenched} = 1 - e^{-\ell/v\tau_s} \qquad (3.6)$$

At a metastable velocity of 10^6 centimeters per second along a one centimeter path in an rf quench region, 85 percent of the metastable are quenched if the energy density of the field is seven milliwatts per square centimeter. This is representative of the parameters of the present experiment.

After passing through the rf quench region most of the metastables which had entered have made transitions to the ground state of the atom and therefore produce no signal when they enter the dc quench field in front of the CEM. Therefore, the signal observed with the rf field on has an enhanced background due to charged particles.

The rf quench region is positioned between the slits (Figures 4 and 5) so that the Lyman α produced by quenching in the rf field cannot reach the detector without making several reflections from walls. The entire path from the excitation region to the detector is enclosed by the grounded 1.0 centimeter I.D. tube, shown in

Figure 5. This shielding eliminates stray fields from the travel path in order to avoid accelerating photoelectrons as well as to avoid quenching of the H(2S) atoms by stray fields.

During the experiment this rf field is alternately turned on and off for equal periods of time, ranging from 5 to 40 minutes. The signal is recorded in both the "quench on" and "quench off" configurations. The background signal is separately determined and can be subtracted from the total signal recorded in the "quench off" condition to yield the metastable contribution alone.

External Magnetic Field Coils

A pair of magnetic field coils, each coil having 500 turns and a mean radius of 11 centimeters, is mounted to the exterior of the vacuum system. The original purposes of this arrangement were to provide increased alignment of electrons in the excitation region and to allow distinction between the signal due to H(2S) atoms and ions by altering the position of the latter in the time-of-flight spectrum by deflection in the magnetic field. The construction of the system with nonmagnetic materials (very low permeability), except for the nickel base material of which the cathode is constructed, made this approach feasible. A coil current of as high as 3 amperes was capable of producing fields of 45 gauss in the region between the electron gun and the CEM for recognition of the signal due to charged

particles. When used for this purpose the magnetic field did not allow identification of background peaks, but did allow noticeable shifting of some background peaks in the time-of-flight spectrum.

Small magnetic fields, less than ten gauss, were applied to the excitation region during data runs to increase alignment of electron paths perpendicular to the electron gun-CEM direction. This technique appears to have increased the resolution in the time-of-flight spectrum: the spread in velocities of the excited molecules in the direction of the detector due to momentum transfer by the bombarding electrons appeared to be decreased.

Timing Electronics

The pulsing logic is shown schematically in the bottom half of Figure 4. Each cycle is initiated by the negative-going portion of one output cycle of a Hewlett-Packard Square Wave Generator, Model 211A, which is operated at 20 kHz. This pulse triggers an E-H Research Laboratories 120D Pulse Generator which generates two simultaneous matched output pulses. These output pulses are variable in amplitude (± 25 volts each), variable in pulse width (0.010 to 0.150 microseconds), and have rise times of the order of two to ten nanoseconds depending on the pulse width and output impedance matching. One of the 120D pulses triggers a second E-H 120D whose output pulses are paralleled through a diode arrangement to provide pulses as large as

-45 volts to the electron gun cathode. The second output pulse of the first 120D trigger is delayed by an E-H Model 921 delay generator, the output of which is then used as the start signal for an Ortec 437A Time to Pulse Height Converter (TPHC). Use of this delay allows the data from the time of interest after excitation to be analyzed and displayed in more channels of the analyzer which comprises the final stage of signal processing, thereby increasing time resolution. The "stop" pulse to the TPHC comes from the CEM via an Ortec Model 109A preamplifier and a single channel analyzer.

The output pulse of the CEM (50 nanoseconds FWHM) is input to an Ortec 109A preamplifier which produces a distribution of output pulses whose maximum is located between 0.3 and 0.4 volts, with a 0.05 microsecond risetime and a decay time of 0.25 microseconds. An uncertainty in timing which is produced by this distribution of signal amplitudes is discussed later in this section. An Ortec Single Channel Analyzer (SCA), Model 406, is used as the discriminator. The SCA produces an output pulse when a given input signal falls below a threshold voltage on the decay of the pulse. The SCA output is the stop signal for the TPHC.

The TPHC produces an output pulse whose voltage is proportional to the time between the start and the stop pulses which have been applied to it. This signal is fed into a Technical Measurement Corporation 400 Channel Analyzer Model 404, for analysis, storage

and display. Since the count rates are all less than 100 counts per second, there is no "pileup" in the system, i.e. no input of one pulse to any component while another pulse is still being processed. The pileup is determined by the longest time that any component in the system requires after an input before it can accept and process another input. In this sytem, the maximum count rate which the analyzer can process is approximately 10^4 counts per second.

The electron gun input pulse which couples inductively as a low level signal in the output of the preamplifier serves as an excellent timing event for checking delays and timing sequences. A Tektronix 545B oscilloscope is used as a constant monitor to display the time delay between the turn-on of the electron gun and the start pulse applied to the TPHC as well as to occasionally check the character of the output of the preamplifier.

The largest error caused by the pulsing and timing system in determining the time-of-flight is due to the manner in which the preamplifier output pulses are discriminated. The pulse height distribution out of the preamplifier is very narrow, i.e., the output pulses are all very similar in amplitude and character. A typical pulse height distribution is presented in Figure 6. The pulse whose peak is just above the minimum discriminator level setting will produce an output whose time delay from the peak of the pulse is very short. However, a pulse which exceeds the threshold by an appreciable voltage

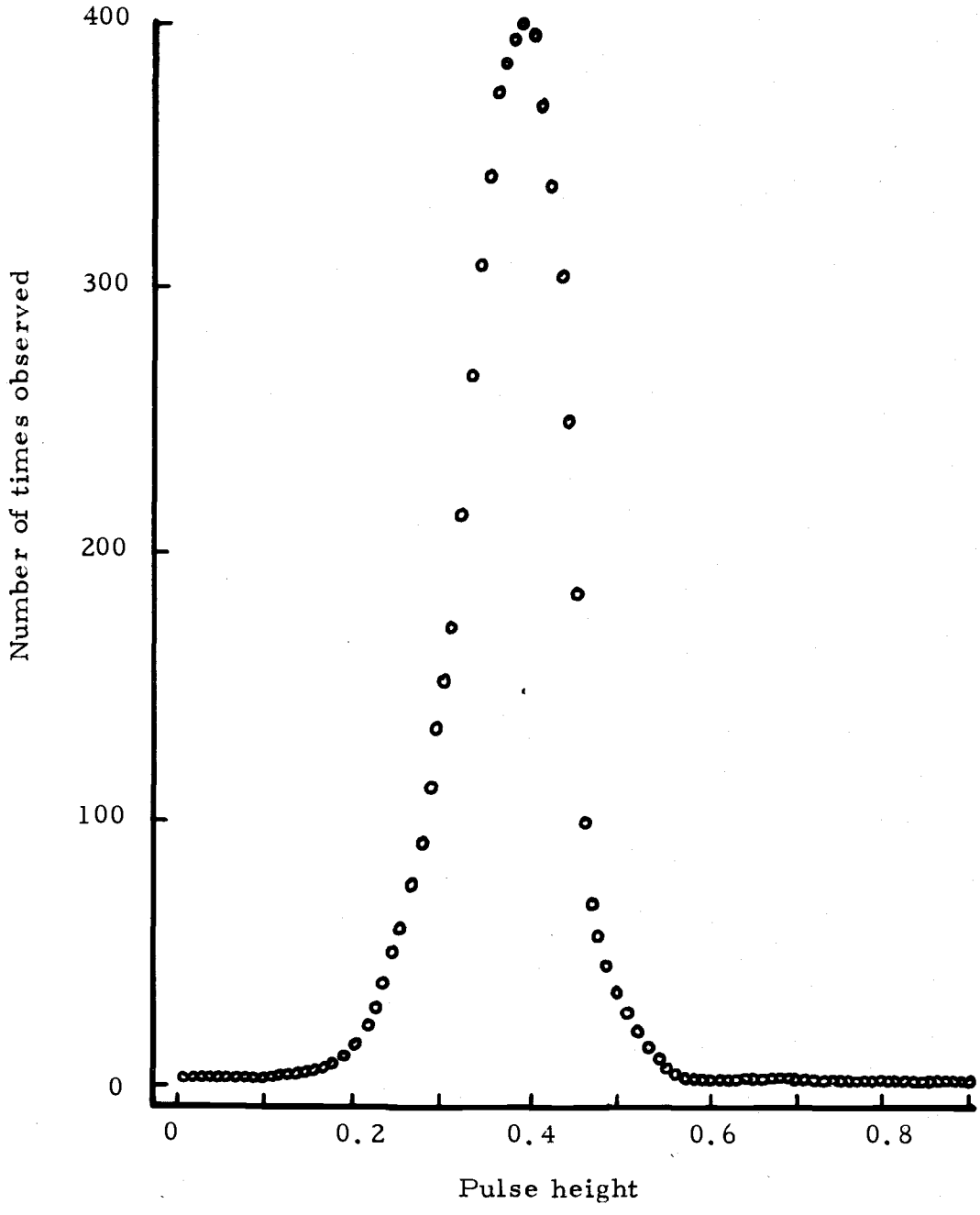

Figure 6. Pulse height distribution of the electron multiplier and preamplifier.

will take longer from the peak to the time at which the voltage level crosses the threshold level again. The resulting output of the SCA for the larger pulse will be correspondingly farther (in time) from the peak of the pulse. This error is at most 0.1 microsecond in the present experiment. The pulse height distribution of the CEM exhibits that practically all pulses are within a factor of two in amplitude. When the discriminator threshold is set to the lower level, the time width of signal of the pulse whose voltage is twice as much as the minimum setting of the SCA is 0.2 microseconds.

CALCULATION OF PREDISSOCIATION RATES

Although the general theory of predissociation was discussed many years ago by Kronig (24), it is only through the use of the digital computer that actual calculations are feasible. This is because the matrix elements are quite sensitive to the wave functions employed. Predissociation rates for some states of H_2 have been computed by Nielsen and Berry (34). These calculations are based on the Hamiltonian and wave functions produced in the Born-Oppenheimer approximation. In the present section we shall review the general method used in calculations of predissociation and identify the perturbations which have been used.

The impetus for performing detailed calculations of the predissociation process has been provided by the results of the high resolution photoionization experiment of Chupka and Berkowitz (9) and an experiment by Comes and Wellern (12). In the latter work predissociation was observed by monitoring the absorption of ultraviolet radiation by H_2 at various wavelengths and detection of the resulting Lyman α emitted by the target gas with and without an electric quench field. Predissociation manifests itself in the absorption spectrum by a broadening of the spectral line of a predissociating level to a greater width than if the excited state decayed solely by radiative decay.

This broadening can be understood in a semi-classical approximation by referring to the form of the transition probability per unit time for absorption of light leading to excitation of one electron and photodissociation in the H_2 molecule:

$$w \alpha \left|(\phi_e(\vec{x}_2, R)\psi_e(\vec{x}_1; R)\chi_e(R, \vec{\theta}) \left|x_{1z}\right| \Phi_g(\vec{x}_2, \vec{x}_1; R)\chi_g(R, \vec{\theta}))\right|^2 \qquad (4.1)$$

in which

ϕ_e = portion of the excited state wave function which describes the unexcited (core) electron.

ψ_e = portion of the excited state wave function which describes the excited electron.

χ_e = vibrational-rotational portion of the wave function for the excited molecular state.

Φ_g = total electronic wave function for the unexcited molecule.

χ_g = vibrational-rotational portion of the wave function for the unexcited molecule.

R = internuclear distance.

$\vec{\theta}$ = coordinates describing the angular orientation of the nuclei.

$\vec{x}_1, \vec{x}_2$ = electron coordinates

The semicolons in equation (4.1) indicate that the internuclear distance R is a parameter in the electronic wave functions. This

particular separation of wave functions and functional dependence is presented in light of the results of the Born-Oppenheimer approximation and the assumption that the effects of the core electron on the excited one can be approximated by an effective core potential which depends on R. The above transition rate can be rewritten as a product of a vibrational-rotational (which will be called Franck-Condon) element and an electronic portion

$$w \alpha \left|(\chi_e(R,\theta)\chi_g(R,\theta))\right|^2 \cdot \left|(\phi_e(x_1, R)\psi_e(x_2; R)\left|x_{2z}\right|\Phi(x_1, x_2; R))\right|^2. \tag{4.2}$$

If the electronic matrix element in equation (4.2) is roughly independent of R over the range of its values which contribute to the transition probability, as determined by the Franck-Condon portion, the dependence of the photodissociation probability upon photon energy is strictly due to the variation of the latter quantity with excitation energy. In Figure 1 the transition labelled 1 is the best suited for this approximation.

Now consider excitation to a bound level associated with a potential curve that is crossed by or lies in close proximity to a dissociating curve, at the energy of the bound state, as shown in Figure 2. In such a case the vibrational wave function which contributes to the Franck-Condon portion of the matrix element is composed of contributions of both the bound level and the unbound vibrational state of the

dissociating curve. It is this perturbation of the original bound vibrational wave function which produces the energy broadening exhibited by some predissociating levels.

The predissociation rates that Nielsen and Berry calculate are for predissociation into $H(1S) + H(n\ell: \ell \geq 3)$. Similar computations for predissociation into $H(1S) + H(2S)$ are more difficult, because of the accuracy required, and have been left for later consideration. Before discussing the perturbations that have been used we shall briefly describe the Born-Oppenheimer method so that the approximations which enter into the calculations of the basis functions will be evident.

The exact Hamiltonian for an H_2 molecule is

$$H = T_e + T_n + U(x_1, x_2, X_1, X_2) \tag{4.3}$$

where T_e and T_n are the electron and nuclear kinetic energy operators, respectively, and U is the potential energy which contains the electron-electron, proton-proton, and electron-proton interactions. The x_1, x_2 in the argument of U are the coordinates of the two electrons. The X_1, X_2 denote the coordinates of the two protons. The kinetic energy operators are

$$T_e = -\frac{\hbar^2}{2m} \sum_{i=1,2} \left(\frac{\partial^2}{\partial x_i^2} + \frac{\partial^2}{\partial y_i^2} + \frac{\partial^2}{\partial z_i^2} \right) \tag{4.4}$$

$$T_n = -\beta^4 \frac{\hbar^2}{2m} \sum_{i=1,2} \left(\frac{\partial^2}{\partial X_i^2} + \frac{\partial^2}{\partial Y_i^2} + \frac{\partial^2}{\partial Z_i^2} \right) \qquad (4.5)$$

where m is the mass of an electron and $\beta^4 = m/M$ is the ratio of the electron mass to the total nuclear mass.

The nuclear kinetic operator is treated as a perturbation. The effective potential energy part of the unperturbed Hamiltonian is chosen to include only the Coulomb monopole, exchange, and quadrupole contributions to the exact Coulomb potential. We designate this approximate potential as $V(x_1, x_2, X_1, X_2)$. The unperturbed Hamiltonian is, in accord with these approximations,

$$H_o = T_e + V(x_1, x_2, X_1, X_2) \ . \qquad (4.6)$$

The form of the unperturbed problem is therefore

$$(H_o - W^o)\Psi^o = 0 \ . \qquad (4.7)$$

A transformation to a coordinate system in which R is the relative coordinate between the two nuclei and $\vec{\theta}$ represents the coordinates of the center of mass and the polar coordinate angles of the line joining the nuclei), facilitates understanding of the solution for the H_2 system. In terms of these coordinates, the unperturbed problem may be written

$$\left[H_o(\vec{x}_1, \vec{x}_2, \frac{\vec{\partial}}{\partial x_1}, \frac{\vec{\partial}}{\partial x_2} \ ; \ R, \vec{\theta}) - W_n(R)\right]\Psi^o(\vec{x}_1, \vec{x}_2; R, \vec{\theta}) = 0 \qquad (4.8)$$

Since the assumption that the nuclear kinetic energy operator is a small perturbation term has been made, the position coordinates of the nuclei appear only as parameters (denoted by positioning after the semicolon in the arguments) in the above equation: for a given set of R and θ a solution is obtained. This parametric dependence is additionally exhibited by the dependence of the eigenvalue W_m on the internuclear coordinate.

An unperturbed molecular wave function Ψ_n^o can be written as a product of three functions.

$$\Psi_n^o = \phi_{el}^o (\vec{x}_1, \vec{x}_2; R) \chi^o(R) \Theta(\vec{\theta}) \tag{4.9}$$

where $\phi_{el}(x_1, x_2; R)$ is the electronic portion of the wave function $\chi_o(R)$ is the molecular vibrational wave function, and $\Theta(\vec{\theta})$ is the rotational wave function. Since the position coordinates of the nuclei are parameters in the unperturbed Schrodinger equation, that expression becomes an equation for the electronic wave function by virtue of the dependence chosen for the functions above:

$$[H_o(\vec{x}_1, \vec{x}_2, \frac{\vec{\partial}}{\partial x_1}, \frac{\vec{\partial}}{\partial x_2}; R, \vec{\theta}) - W_n(R)]\phi_{ei}^o(\vec{x}_1, \vec{x}_2; R) = 0 \tag{4.10}$$

In order to determine the vibrational and rotational wave function it is necessary to continue the expansion of the Hamiltonian and wave function in terms of the parameter β. (The justification for the use of β instead of β^4 or another power of β is not evident in this

presentation, but it allows for expansion of the operators and wave functions in terms of ascending powers of β. In the detailed analysis this provides ease in collecting terms and separating out the perturbation equations in powers of β.) The nuclear kinetic energy operator, in terms of the new coordinates, is

$$T_n = -\beta^4 \frac{\hbar^2}{2m} \{4 \frac{\partial^2}{\partial R^2} + \frac{8}{R} \frac{\partial}{\partial R} + \Delta_o + \frac{4}{R^2} \Delta_\theta\} \quad (4.11)$$

where

$$\Delta_\theta = \frac{1}{\sin\theta} \frac{\partial^2}{\partial \omega^2} + \frac{1}{\sin\theta} \frac{\partial}{\partial \theta} (\sin\theta \frac{\partial}{\partial \theta}) \quad (4.12)$$

$$\Delta_o = \frac{\partial^2}{\partial X_o^2} + \frac{\partial^2}{\partial Y_o^2} + \frac{\partial^2}{\partial Z_o^2} \quad (4.13)$$

and θ and ω are the polar coordinates of the line joining the nuclei. Use of this nuclear kinetic energy operator and the usual procedures of Rayleigh-Schrodinger perturbation theory produces a differential equation for the zeroth order vibrational wave function in which derivatives of the unperturbed eigenvalues, $W_n(R)$, are force constants. The succeeding approximation then determines the rotational wave function. The most important point for our present discussion is that nowhere in the determination of the lowest order total wave function are any derivatives of $\phi^o_{ei}(x_1, x_2; R)$ taken with respect to the nuclear coordinates.

The most obvious operators that could be selected to couple

the states generated in the above process are the noncentral (with regard to the molecular system) portion of the Coulomb interaction, the spin-orbit interaction, and the nuclear kinetic energy operator. The noncentral portion of the Coulomb interaction has been used as a perturbation in calculations of autoionization (37). Predissociation in the oxygen molecule has been interpreted in terms of the spin-orbit interaction (32). However, since predissociation occurs by means of a transition from a bound vibrational state to an unbound vibrational state, the nuclear kinetic energy operator is the most prominent candidate as the important coupling operator in the majority of cases of predissociation.

Nielsen and Berry describe the electronic wave function denoted by ϕ^{o}_{el} above, as a product of a wave function, $\Phi(\vec{x}_2; R)$ that describes the core electron and a one-electron wave function, $\psi_n(\vec{x}_1; R)$, that describes the active electron,

$$\phi_{el}(\vec{x}_1, \vec{x}_2; R) = \Phi(\vec{x}_2, R)\psi_n(\vec{x}_1; R), \qquad (4.14)$$

This separation of the electronic wave function is justified by the observations of band systems in H_2 (19, p. 323). The energy levels and spacings of these systems correspond well with calculations based on a one-electron excited state in which the second (unexcited) electron provides a contribution to a "core potential" which is altered only slightly with different levels of the excited electron. Such states

which have only one electron excited are called Rydberg states.

This separation of the electronic part of the wave function allows the Born-Oppenheimer problem to be converted to a one-electron problem if the effect of the core function is included in some average manner in the potential so that $H_o(\vec{x}_1, \vec{x}_2, R, \vec{\theta})$ is replaced by $H'_o(\vec{x}_2, R, \vec{\theta})$, and

$$[H'_o - W'_n(R)]\psi'_n(\vec{x}_2; R) = 0. \tag{4.15}$$

The perturbation operator used by Nielsen and Berry is the $\frac{\partial^2}{\partial R^2}$ term of the nuclear kinetic energy operator. The major contribution to predissociation comes from the matrix element

$$T'_n = -2\beta^4 \frac{\hbar^2}{m}(\psi_f \chi^o_f \left| \frac{\partial \psi_i}{\partial R} \frac{\partial \chi^o_i}{\partial R} \right.) \tag{4.16}$$

where the subscripts i and f denote the initial and final states, respectively. The rotational part of the kinetic energy operator is not treated in the work of Nielsen and Berry.

Evaluation of the matrix element in equation (4.16) demonstrates that the transition amplitude can accumulate over a large range of internuclear separation R. This contrasts with the usual Franck-Condon assumption which is made in discussing direct dissociation that transition amplitudes accumulate principally at the classical turning points. This discovery leads to the conclusion that predissociation may occur from high vibrational levels of one Rydberg state

(one-electron excited) into the vibrational continuum of a lower state by a radiationless transition.

Predissociation transition rates as high as 10^{12} per second have been calculated by Nielsen and Berry for transitions between low lying levels of H_2. As an example, in the decay of the $8p\sigma(v=3)$ state predissociation into an unbound $5p\sigma$ vibrational state to produce $H(1S) + H(3S)$, predissociation is the predominant decay process with a rate of 10^{11} per second. Rates which are this high allow predissociation to compete with and predominate over autoionization and radiative decay as a decay mechanism for several excited states of the H_2 molecule.

EXPERIMENTAL RESULTS

The interpretation that predissociation is the primary mechanism for the production of H(2S) atoms in electron bombardment of H_2 is based on observation of peaked structure in the time-of-flight distribution of the H(2S) atoms. The effect of cooling the target gas on the resolution of these peaks is demonstrated by comparing the distributions of Figures 8 and 9 with that in Figure 7. When H_2 is delivered to the excitation region at temperatures above 80° K distributions similar to that shown in Figure 7 are observed. This result is qualitatively the same as those obtained by other investigators (10, 11, 27). In contrast, when the gas is cooled to a temperature less than 60° K (recall Chapter 3 and Appendix A) structure of the type shown in Figures 8 and 9 appears. Figure 9 represents the data of one of eight low temperature runs from which the peak locations listed in Table 1 were obtained. Channel numbers are provided in Table 1 to allow location of the peaks in Figure 9.

The relative amplitudes of various peaks in the time of flight distribution depends upon the electron excitation energy. All of the peaks listed in Table 1 are not clearly evident, but the structure present at channels 43, 80 and 128 is easily recognizable. The positions of the peaks in the time-of-flight distribution are independent of electron excitation energy. However, at different electron

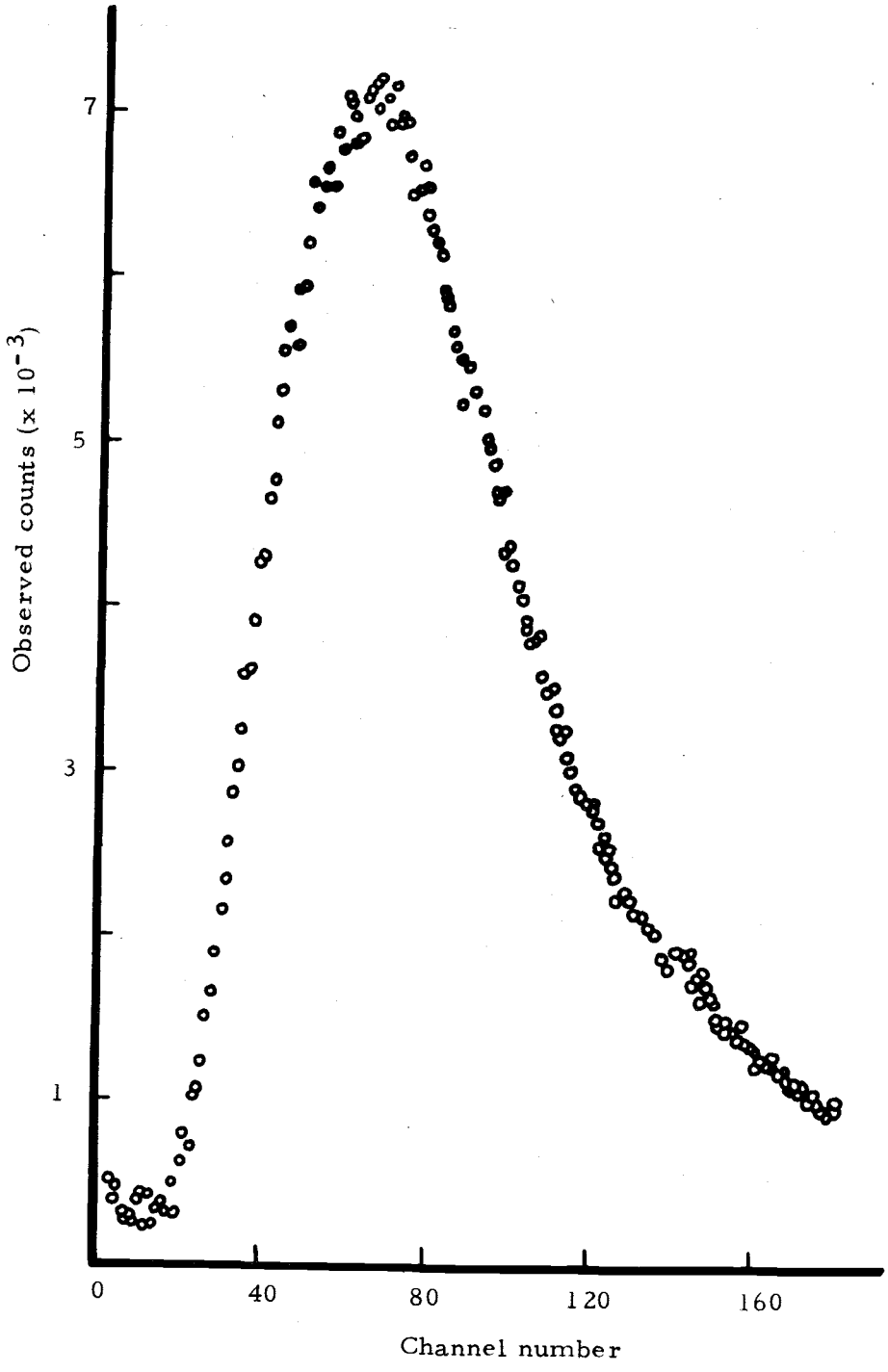

Figure 7. Time of flight distribution at a temperature greater than 80° K. Channel 0 corresponds to 4.48 microseconds after excitation. Each channel represents 0.107 microseconds. The entire range shown is from 4.48 to 24.48 microseconds. These data were taken at a pressure of 4×10^{-5} torr of H_2 with an electron gun pulse of -38 volts, 0.06 microseconds FWHM.

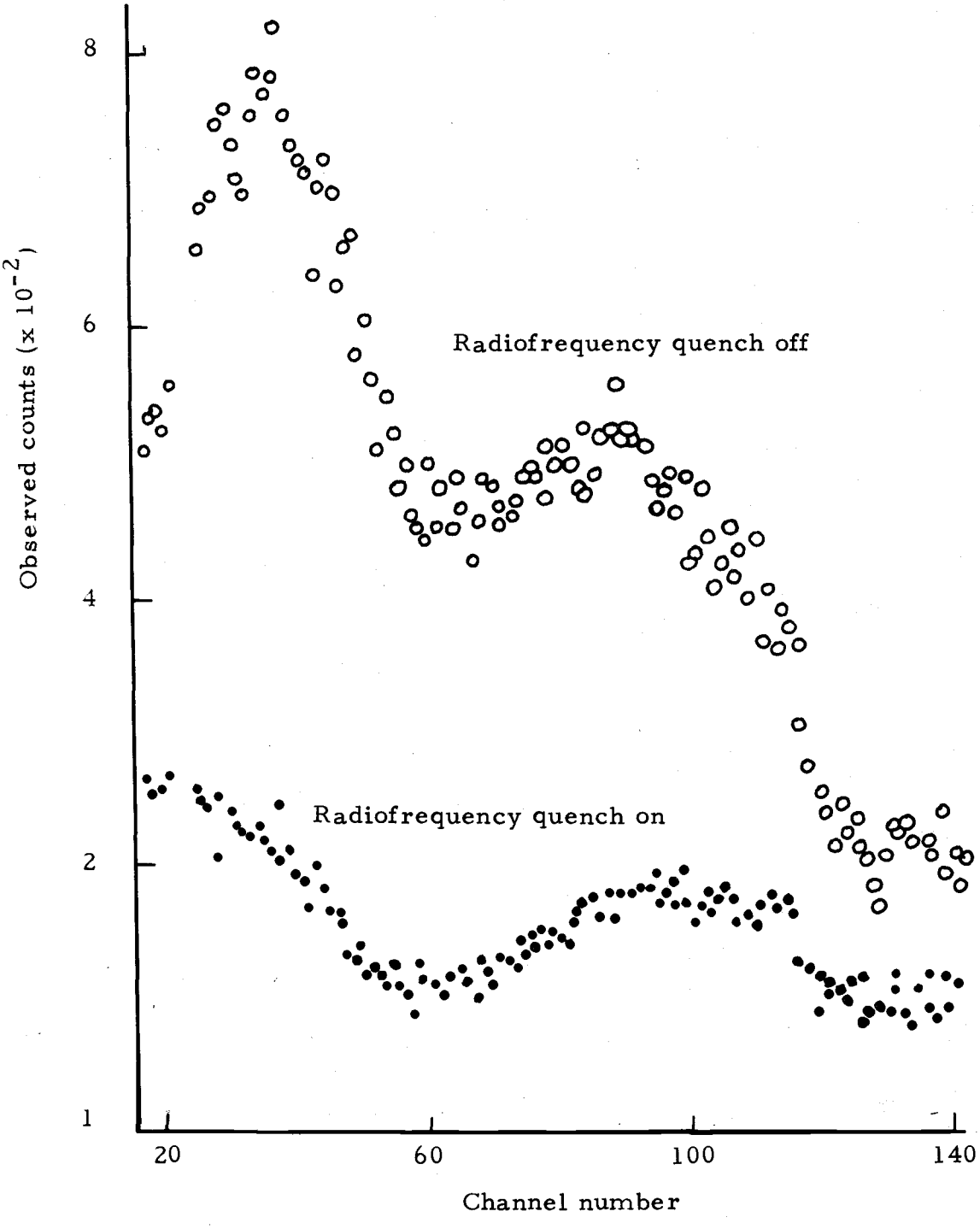

Figure 8. Time of flight data at a temperature less than 60° K. Both background (quench on) and total signal are shown. The data in a few channels affected by identifiable spurious (inductive) effects have been deleted. The target gas pressure is 0.6×10^{-4} torr.

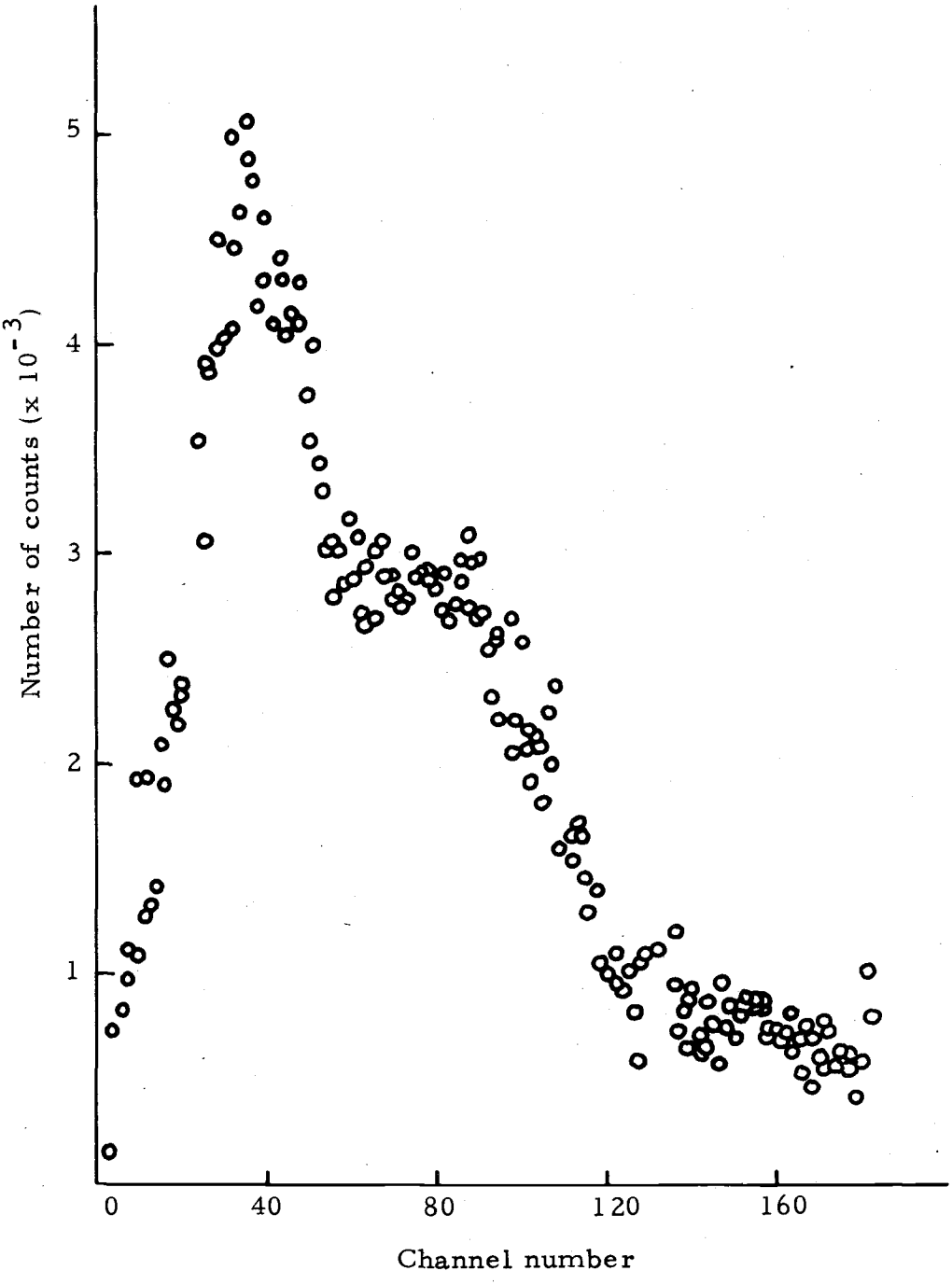

Figure 9. Time of flight distribution at a temperature less than 60° K. These points were obtained from the data partially displayed in Figure 8 by subtracting, channel by channel, the rf quench on from the rf quench off data. Each channel represents 0.107 microseconds. Channel 0 corresponds to a time-of-flight of 4.6 microseconds.

Table 1. Location and identifcation of peaks in the H(2S) time-of-flight spectrum.

Location in Time (usec)	Channel Number (Fig. 9)	H (2S) Kinetic Energy (eV)	Excitation Energy (A)	Optical Absorption Feature (A)	Predissociating Levels	Dissociation Curves
8.4	35	0.86	753 ± 4[a]	753.3[b] 755.6[b]	$9p\sigma\ ^1\Sigma_u^+(v=5)$ $8p\sigma\ ^1\Sigma_u^+(v=5)$	$(2s\sigma)(2p\sigma)\ ^1\Sigma_u^+$
9.3	43	0.68	768 ± 4	765.4[b]	$8p\sigma\ ^3\Sigma_u^+(v=4)$	$(2s\sigma)(2p\sigma)\ ^3\Sigma_u^+$
13.4	80	0.34	807 ± 2	805[c]	$D\ ^1\Pi_u(v=6)$	$B'\ ^1\Sigma_u^+$
15.4	98	0.26	817 ± 1	816[c]	$D\ ^1\Pi_u(v=5)$	$B'\ ^1\Sigma_u^+$
18.7	128	0.17	827 ± 0.5	827[c]	$D\ ^1\Pi_u(v=4)$	$B'\ ^1\Sigma_u^+$
21.3	152	0.13	830 ± 0.5	839[c]	$D\ ^1\Pi_u(v=3)$	$B'\ ^1\Sigma_u^+$

[a] These uncertainties are discussed in the text.

[b] Ref. 9. The first and third of these features are abnormally broad autoionization peaks; the second feature is a missing autoionization peak.

[c] Refs. 11, 12, 27, 39. These features are peaks in both optical absorption and photodissociation spectra.

[d] The triplet level listed here should be nearly degenerate with the singlet level observed in optical absorption (8). This tentative identification is made because the calculated (22) energy separation between the two repulsive curves at the curve crossing position is approximately equal to one vibrational quantum, at this excitation energy.

energies various peaks are not resolvable because of changes in the relative amplitudes.

The kinetic energy of the metastables is calculated according to Equation (1.2), $E = mL^2/2t^2$, directly from the time-of-flight indicated by the various peaks. Since the distribution which the metastables in any peak exhibit is quite narrow, the transformation from the time-of-flight distribution to the energy distribution was not applied. The shift in the location of the energy maximum caused by this transformation is very small compared to other errors, especially that due to the uncertainty in path length.

The excitation energy, which is expressed in Angstroms in Table 1, is calculated according to Equation (1.4). It is assumed that the H(2S) atoms are produced by predissociation of an excited molecule, which is at rest in the laboratory, into an atom in the ground state and one in the 2S state. The error presented in the fourth column of Table 1 is the error due to the uncertainty in locating the points of production and detection of the metastables, under the assumption that the excited level identification is correct. The maximum possible uncertainty in the kinetic energy of the metastables is 18 percent due to this location uncertainty, but the distribution of path lengths must be quite peaked at some value within the limits 10.8 ± 0.5 cm in order to allow resolution of the structure observed. Resolution in the timing circuitry, as discussed in Chapter III, can

produce a maximum error of two percent in the determination of the kinetic energy of the metastables. Contributions to error due to the kinetic energy of the excited molecules prior to predissociation are ignored since this energy is less than 0.004 ev if the molecules are at 50°K.

The designation of the "excitation energy" disregards the possibility that some of the metastables may have been created by cascade from atoms produced by dissociation into higher atomic states. The contributions of H(2S) from cascading as determined from calculated transition probabilities is small. The most likely parent states, the 3P states of H, have a $3P \rightarrow 1S$ transition probability which is seven times the value of the $3P \rightarrow 2S$ transition probability (14, p. 134).

Since relatively little is known about the higher-lying potential curves of the H_2 molecule, these assignments of excitation energies, predissociating levels, and dissociation curves, as presented in Table 1, are merely indications of the probable origins of the H(2S) atoms. The correlations of these results with the observations of other investigators, which is discussed below, present arguments for the particular designations that are indicated in Table 1 for the origins of the observed structure.

The peaks at 13.4, 15.4, 18.7 and 21.3 microseconds correspond to the well known predissociation of the $D^1\Pi_u$ (v=3, 4, 5, 6) levels by the $B'^1\Sigma_u^+$ repulsive potential states. Predissociation of

the $D^1\Pi_u$ levels has been observed by line broadening in absorption spectra (33, 37) and by simultaneous optical absorption and observation of Lyman α produced when a dc electric field is applied to the excitation region (12, 13).

All of the low temperature data exhibit signal but no clearly evident structure in the region between channels 45 and 70 in Figure 9. This may result from H(2S) atoms produced by direct excitation to the dissociation continuum. Predissociation of the $D^1\Pi_u$ (v=7) levels (9, 29) can be expected to produce a feature at 795 A (channel 69 in Figure 7). Either of these processes can reasonably contribute to the observed signal. A combination of the two is the most likely interpretation unless there is some unknown predissociating level which contributes to the signal in this range.

Anomalous broadening of the absorption line at 765.4 A has been attributed (9) to exceptional autoionization of the $8p\sigma$ (v=5) Rydberg state of H_2. Since the energy of this level corresponds with the peak at 9.3 microseconds (768±4A) in Table 1, it appears that some of the anomalous broadening may be ascribed to predissociation which occurs in addition to autoionization. Some of this signal is probably due to the singlet state, $8p\sigma\,^1\Sigma_u^+$. The particular choice of the triplet state in Table 1 is discussed below.

The interpretation of the peak at 8.4 microseconds is complicated by the estimated experimental error and the possibility that

one or both of two states may be predissociating to produce this structure. An anomalously broad absorption line which has been attributed to the $9p\sigma$ ($v=5$) Rydberg state which occurs at 735.3 A (9). There is also a "missing" absorption line at 755.6 which is associated with the $8p\sigma$ ($v=5$) state. It has been conjectured that this line is broadened beyond recognition by autoionization of this level. In order that it autoionize, the $8p\sigma$ ($v=5$) state must undergo a transition to an ion in the $v=4$ vibrational state and a free electron. The operation of a propensity rule that such autoionization rates (and also the corresponding broadening of associated absorption lines) decrease with increasing $|\Delta v|$ has been proposed theoretically (3) and observed experimentally in H_2 (9). Since nearby states in H_2 follow this rule consistently, it is unlikely that the line at 755.6 is broadened beyond recognition by autoionization alone because the states which predissociate by a transition with $\Delta v=1$ are observable. With the present evidence it is not possible to distinguish whether one or both of these levels are producing the peak at 8.4 microseconds in the time-of-flight distribution.

The assignment of dissociation curves for the peaks at 8.4 and 9.3 microseconds have been made in accordance with the selection rules for predissociation in H_2 (19, p. 416)

$$\Delta J = 0 \qquad \Delta S = 0 \qquad \Delta \Lambda = 0, \pm 1 \tag{5.1}$$

where J is the total angular momentum, S is the total spin, and Λ is the projection of electronic orbital angular momentum on the internuclear axis. The character of the dissociating curve, except for the total spin quantum number, is determined by the selection rules. The configuration $(2s\sigma)(2p\sigma)$ is the lowest energy molecular configuration lying above the $(1s\sigma)(2s\sigma)\, B^1\Sigma_u^+$ that can dissociate into an atom in the ground state and one in the 2S state. At these energies the singlet and triplet $8p\,\Sigma_u^+$ levels should be nearly degenerate. The calculated splitting between the repulsive singlet and triplet $(2s\sigma)(2p\sigma)\,{}^1\Sigma_u^+$ levels is approximately equal to one vibrational quantum (22). Therefore the choice of the triplet levels as the states associated with the peak at 9.3 microseconds allows for a consistent perturbation of the two vibrational levels of the $8p\sigma$ states by two repulsive potential curves which have similar energy spacing.

Recent data and comments concerning the angular distribution of H(2S) atoms and the symmetry properties of the predissociating states have suggested that other states, such as the $d^3\Pi_u^+$ and $e^3\Sigma_u^+$ may be contributing to the observed structure (30). At present there is no means of conclusively determining which states are contributing to the predissociation observed. In general, singlet-triplet excitation occurs by exchange and its cross-section is strongly peaked near threshold (15, 35). Singlet-singlet excitation occurs by

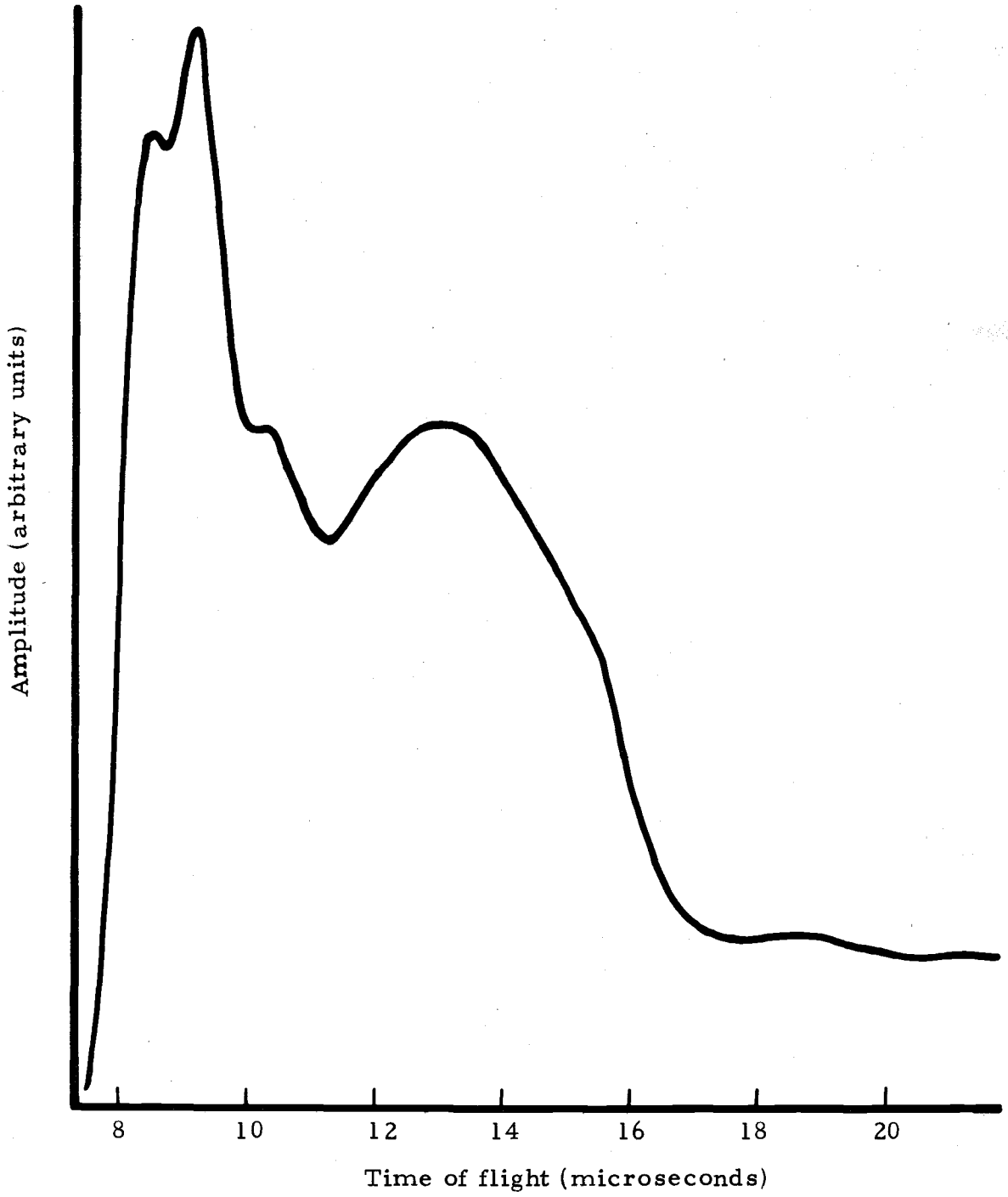

Figure 10. Time of flight distribution produced by using the times of the experimentally observed peaks in the theory of Stanton and Monahan. Two additional peaks have been added at 10.5 and 11.9 microseconds in order to produce a contribution comparable to the evident but unresolved features in Figure 9 between channels 45 and 70.

direct excitation and the cross-section for this process increases for several volts above the initial excitation energy for the excited singlet state threshold and then slowly decreases (36). No rapid variation in the relative peak amplitudes of the structure was observed here.

The consistency of the assumptions concerning the narrow energy width of the predissociating levels and the temperature effects is demonstrated by Figure 10; there, a linear combination of the functions given in Equation (2.7), with appropriate coefficients and the times-of-flight listed in Table 1, are plotted. Two peaks have been inserted between the peaks at 9.3 and 13.4 microseconds in order to simulate the data of Figure 9 in the region between channels 45 and 70.

DISCUSSION

The correspondence of the structure in the time-of-flight distribution to the known predissociating levels and to unusually broadened or missing lines in absorption spectra indicates that the production by electron bombardment of H(2S) atoms with kinetic energies between 0.13 ev and 0.86 ev occurs primarily through predissociation. The $D^1\pi u$ (v = 3, 4, 5, 6) appear to produce a large fraction of the H(2S) atoms observed in this energy range. It is indicated that there is an appreciable contribution of H(2S) atoms from predissociation of the Rydberg state, $8p\sigma$ (v=4), and one or both of the states, $8p\sigma$ (v=5) and $9p\sigma$ (v=5), which has not been previously reported. This latter observation agrees with the general tenor of the theoretical calculations of Nielsen and Berry: autoionization and predissociation are competing process for decay of some of the Rydberg states of H_2.

Although the interpretation of the structure in the time-of-flight spectrum has been based on other experimental observations with good correspondence, it is important to emphasize here that this interpretation is only well indicated, not proven.

It has been reported that there are resonances in the photodissociation continuum of diatomic molecules when the excitation is to a repulsive portion of a potential energy curve which has some bound

states occurs (6). This may add further complications to interpretation of data such as that presented in this experiment. At the present time the calculations of this structure for the oxygen molecule indicate that such structure is too broad and weakly pronounced to be of significance here. It appears that, in the excitation energy range used in this experiment, such structure in the dissociation of H_2 cannot be detected by a time-of-flight method because of the predominance of predissociation.

The limit of useful temperature reduction for the target H_2 molecules has been attained. The recoil from the excitation provides a spread in H(2S) velocities which is adequate to account for the width of the structure in the time-of-flight spectrum. A more directional electron gun may allow increased resolution of the structure reported here, but such a change would not yield sufficient additional resolution to justify the alterations. If the "fast" metastables (which were not considered in the present investigation) are really dissociation products of doubly excited molecular states, structure due to a kind of predissociation may be available with proper choice of path length and suppression of the photon background from the excitation region.

Predissociation in HD and D_2 of states which correspond to those discussed in H_2 can be expected, according to Berry and Nielsen (34), if the identification of the predissociating Rydberg states

in H_2 has been correct. However, since the predissociation rates depend so critically upon wave functions and energy levels of the states involved, the yields of metastables from corresponding states in HD and D_2 are probably different than those of H_2.

The present work demonstrates the contribution of predissociation of several states in H_2 to the production of metastable H(2S) atoms following electron excitation of the molecule. In light of this discovery, more investigations of the extent to which predissociation affects the dissociation process should be made.

BIBLIOGRAPHY

1. Barbier, D. Airglow. In: Research in geophysics, ed. by Hugh Odishaw. Cambridge, Massachusetts. The M. I. T. Press, 1964. p. 401-407.

2. Becker, E. W. and K. Bier. Die Erzeugung eines intensiven, teilweise monochromatisierten Wasserstoff-Molekularstrahles mit einer Laval-Düse. Zeitschrift für Naturforschung 9A: 975-986. 1954.

3. Becker, E. W., K. Bier and W. Henkes. Strahlen aus kondensierten Atomen und Molekeln im Hoohvakuum. Zeitschrift für Physik 146:333-338. 1956.

4. Berry, R. Stephen. Ionization of molecules at low energies. The Journal of Chemical Physics 45:1228-1245. 1966.

5. Bethe, Hans Albrecht and Edwin E. Salpeter. Quantum mechanics of one- and two-electron atoms. New York, Academic Press, 1957. 368 p.

6. Bixon, Mordechai, Baruch Raz and Joshua Jortner. Resonances in the photo dissociation continuum of diatomic molecules. Molecular Physics 17:593-601. 1969.

7. Born, M. and J. R. Oppenheimer. Zur Quantentheorie der Molekeln. Annalen der Physik 84. 4:457-484. 1927.

8. Chamberlain, Joseph W. The geocorona. In: Research in geophysics, ed. by Hugh Odishaw. Cambridge, Massachusetts, The M. I. T. Press, 1964. p. 189-196.

9. Chupka, W. A. and J. Berkowitz. High-resolution photoionization study of the H_2 molecule near threshold. The Journal of Chemical Physics 51:4244-4268. 1969.

10. Clampitt, R. H(2S) atoms produced by dissociative excitation of molecules. Physics Letters 28A:581-582. 1969.

11. Clampitt, R. and Amos S. Newton. Metastable species produced by electron excitation of N_2, H_2, N_2O, and CO_2. The Journal of Chemical Physics 50:1997-2001. 1969.

12. Comes, F. J. and H. O. Wellern. Die Spektroskopie des Wasserstoffmoleküls in der Nähe seiner Ionisierungsgrenze. Zeitschrift für Naturforschung 23A:881-887. 1968.

13. Comes, F. J. and U. Wenning. Photoinduzierte Stossprozesse metastabiler Wasserstoffatoms mit H_2 im Energiebereich von 0,05 -- 0,47 eV. Zeitschrift für Naturforschung 24A:587-596. 1969.

14. Condon, E. U. and G. H. Shortley. The theory of atomic spectra. Cambridge, Massachusetts, The University Press, 1964. 441 p.

15. Craggs, J. D. and H. S. W. Massey. The collisions of electrons with molecules. Section 2. Excitation of hydrogen. In: Encyclopedia of physics. Vol. 37/1. Berlin, 1959. p. 339-344.

16. Feuer, P. and C. Osburn. Quantum theory of light diatomic gases. In: Rarified gas dynamics, ed. by Leon Trilling and Harold Y. Wachnan, Vol. 2, New York, Academic Press, 1969. p. 1095-1104.

17. Fite, Wade L. and R. T. Brackmann. Collisions of electrons with hydrogen atoms. II. Excitation of lyman-alpha radiation. Physical Review 112:1151-1156. 1958.

18. Harriman, John Martin. Analysis of two problems arising in measurements of hydrogen fine structure. Doctoral dissertation. Palo Alto, Stanford University, 1956. 45 numb. leaves.

19. Herzberg, Gerhard. Molecular spectra and molecular structure. 2d ed. Englewood Cliffs, New Jersey, D. Van Nostrand Company. 1950. 658 p.

20. Huang, Kerson. Statistical mechanics. New York, John Wiley & Sons. 1963. 470 p.

21. Kantrowitz, Arthur and Jerry Grey. A high intensity source for the molecular beam. Part I. Theoretical. The Review of Scientific Instruments 22:328-332. 1951.

22. Kemble, E. C. and C. Zener. The two quantum excited states of the hydrogen molecule. Physical Review 33:512-537. 1929.

23. Kistiakowsky, G. B. and William P. Slichter. A high intensity source for the molecular beam. Part II. Experimental. The Review of Scientific Instruments 22:333-337. 1951.

24. Kronig, R. de L. Zur Deutung der Bandenspektren II. Zeitschrift für Physik 50:347-362. 1928.

25. Lamb, Jr., Willis E. and Robert C. Retherford. Fine structure of the hydrogen atom. Part I. The Physical Review 79:549-572. 1950.

26. Leventhal, M., W. F. Lamb, Jr., K. R. Lea, S. L. Kaufman and D. L. Mader. New methods for measuring hydrogenic fine structure. In: Bulletin of the American Physical Society. New York, 1965. p. 458.

27. Leventhal, M., R. T. Robiscoe and K. R. Lea. Velocity distribution of metastable H atoms produced by dissociative excitation of H_2. Physical Review 158:49-56. 1967.

28. Liepmann, Hans W. and Allen E. Puckett. Introduction to aerodynamics of a compressible fluid. New York, John Wiley & Sons. 1947. 262 p.

29. Mentall, J. E. and E. P. Gentieu. Lyman-α florescence from the photodissociation of H_2. The Journal of Chemical Physics 52:5641-5645. 1970.

30. Misakian, Martin. Research Assistant, University of Michigan, Dept. of Physics. Personal communication. Ann Arbor, Michigan. February 22, 1971.

31. Morack, John Ludwig. Measured lifetimes for the first excited $J = 1(^3P_1)$ level in argon and krypton. Doctoral dissertation. Corvallis, Oregon State University, 1969. 94 numb. leaves.

32. Murrell, J. N. and J. M. Taylor. Predissocation in diatomic spectra with special reference to the Schumann-Runge bands of O_2. Molecular Physics 16:609-621. 1969.

33. Namioka, Takeshi. Absorption spectra of H_2 in the vacuum-ultraviolet region. III. Potential-energy curves for the $B\,^1\Sigma_u^+$, $C\,^1\Pi_u$, $B'\,^1\Sigma_u^+$, and $D'\,^1\Pi_u$ states. The Journal of Chemical Physics 43:1636-1644. 1965.

34. Nielsen, S. E. and R. S. Berry. Vibronic autoionization and predissociation in hydrogen. Chemical Physics Letters 2:503-506. 1968.

35. Prok, George M., Carl F. Monnin and Henry J. Hettel. Estimation of electron impact excitation cross sections of molecular hydrogen. Cleveland, Ohio, 1967. (NASA Technical Note. NASA TN D-4004)

36. _____ Molecular hydrogen inelastic electron impact cross sections--a semiclassical method. Quantitative Spectroscopy and Radiative Transfer 9:361-369. 1969.

37. Russek, A., M. R. Patterson and R. L. Becker. Autoionization in molecular systems. Physical Review 167:17-25. 1968.

38. Smith, Jr., Joe N. and Wade L. Fite. Reflection and dissociation of H_2 on tungsten. The Journal of Chemical Physics 37:898-904. 1962.

39. Stanton, H. E. and J. E. Monahan. On the kinetic-energy distribution of fragment ions-produced by electron impact in a mass spectrometer. The Journal of Chemical Physics 41:3694-3702. 1964.

40. Stickney, Robert E. Atomic and molecular scattering from solid surfaces. In: Advances in atomic and molecular physics, ed. by D. R. Bates and Immanual Estermann, Vol. 3. New York, Academic Press, 1967. p. 143-204.

41. Takezawa, Sanzo. Absorption spectrum of H_2 in the vacuum-uv region. I. Rydberg states and ionization energies. The Journal of Chemical Physics 52:2575-2590. 1970.

42. Tinsley, Brian A. Reinterpretation of geocoronal observations with increased high/low altitude hydrogen ratio. Planetary and Space Science 17:769-771. 1969.

43. Vroom, D. A. and F. J. deHeer. Production of excited atoms by impact of fast electrons on molecular hydrogen and deuterium. The Journal of Chemical Physics 50:580-591. 1969.

APPENDICES

APPENDIX A

ENERGY DISTRIBUTION OF DISSOCIATING ATOMS

The validity of Equations (2.3) and (2.4), the expressions for the energy distribution of dissociated atoms produced with one dissociation energy, Q, from molecules which have a single translational energy, E_M, is demonstrated in this Appendix.

Assume a fixed velocity for the parent molecule

$$V = \sqrt{\frac{E_M}{m}} \tag{A.1}$$

where E_M is the translational energy of the H_2 molecule and m is the mass of one hydrogen atom. The velocity of one dissociated atom in the center of mass system is

$$v = \sqrt{\frac{Q}{m}} \tag{A.2}$$

where Q is the kinetic energy (at infinite separation) imparted to the two atoms in the dissociation process. If the dissociation is isotropic in the center of mass system, the number of atoms produced with the single velocity in a range of angles from θ to $\theta + d\theta$, where θ is an angle measured from an arbitrary z-axis, is

$$dN(\theta) = \frac{\sin\theta \, d\theta}{2} \quad . \tag{A.3}$$

If the velocity of the molecule is directed along an arbitrary z-

axis and a dissociating atom has a velocity v at an angle θ in the center of mass system, the square of the velocity of the atoms in lab system, v_ℓ^2, is

$$V_\ell^2 = V^2 + v^2 + 2vV\cos\theta \tag{A.4}$$

The energy of the atom is

$$E = \frac{1}{2}mv_\ell^2 = \frac{1}{2}m(V^2 + v^2 + 2vV\cos\theta) \tag{A.5}$$

In the range of angles between θ and $\theta + d\theta$, the range of energies dE is

$$dE = -mvV\sin\theta d\theta \tag{A.6}$$

Through the use of the above equation and a transformation of variables, the number of dissociated atoms which have energies between E and $E+dE$ is

$$dN(E) = dN(\theta)\frac{d\theta}{dE} \tag{A.7}$$

or, explicitly

$$dN(E) = \frac{1}{2mvV}(-dE) \tag{A.8}$$

In terms of the kinetic energy of the molecules, E_M and the dissociation energy Q in equations (A.1) and (A.2), the number of dissociated atoms is

$$dN(E) = \frac{1}{2(E_M Q)^{\frac{1}{2}}}(-dE) \tag{A.9}$$

which exhibits the energy distribution presented in equation (2.3). The limits over which the distribution is nonzero are E+ and E- which are defined by equation (A.4) for $\theta = 0$ and $\theta = \Pi$, respectively:

$$E_{\pm} = \tfrac{1}{2} m (V \pm v)^2 \qquad (A.9)$$

In terms of the energy of the original molecules, E_M, and the excess energy in the center of mass system after dissociation, Q, the limits are

$$E_{\pm} = \tfrac{1}{2} (E_M^{\frac{1}{2}} \pm Q^{\frac{1}{2}})^2 \qquad (A.10)$$

APPENDIX B

In this Appendix, an example is presented to demonstrate the relation between effective temperature and kinetic energy of mass flow as the quantities relate to isentropic expansion of gas in a tube (a Laval nozzle).

A cross section of a tube is presented in Figure 11. The upper and lower walls slope apart to the right. The front and back walls (parallel to the plane of the figure) are assumed to be parallel, a distance b apart. There is a pressure gradient to the right in Figure 11, but no gradient in the direction perpendicular to the plane of the figure. Consider a unit mass of gas contained in a volume $v = a \cdot \delta\ell \cdot b$ which is at the left of the tube at time $t=0$. Some time later, at $t=t_1$, the gas has flowed to the right and is contained in the volume v'. Since the expansion is assumed to be adiabatic, the work done on the gas must be equal to the gain in the internal energy of the gas. In calculating the work done and the energy change, the flow and expansion of the gas will be treated separately: the motion of the original amount of gas to the right at constant pressure, then a pure expansion to the volume v'.

During the mass motion, the work done on the gas is

$$\begin{aligned} dw_1 &= -a \cdot b \cdot \delta p \cdot ds \\ &= -\frac{\delta p}{\delta \ell} v ds \end{aligned} \tag{B.1}$$

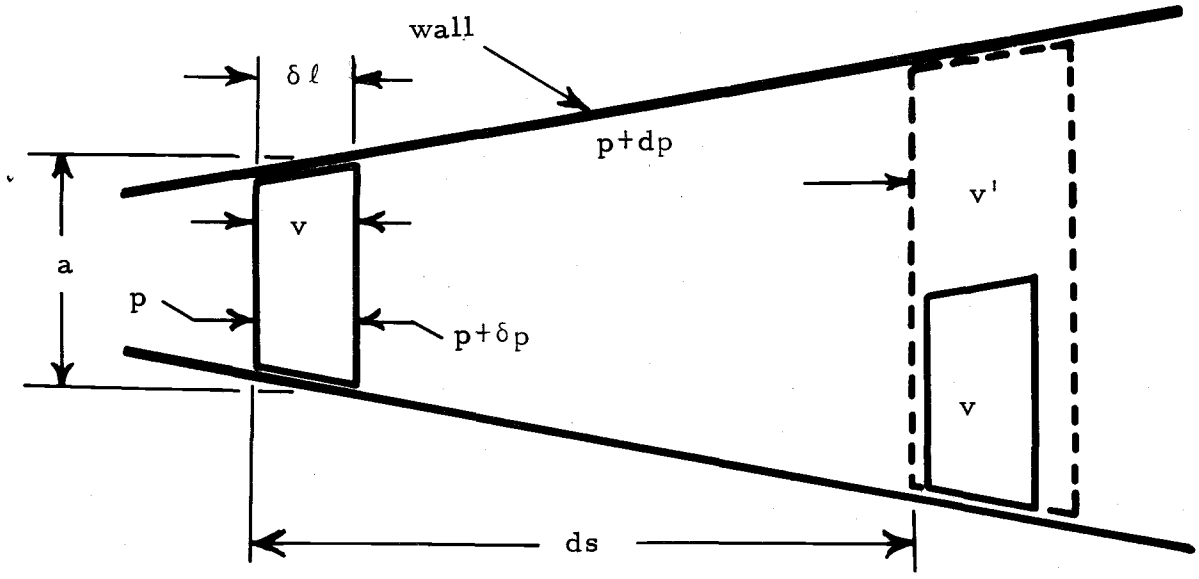

Figure 11. Expansion and flow of a compressible gas in a divergent channel. See text for discussion of the symbols in the figure, the expansion process, and the effective cooling of the gas.

For a constant pressure gradient,

$$\frac{\delta p}{\delta \ell} = \frac{dp}{ds} \tag{B.2}$$

so that

$$dw_1 = - \frac{dp}{ds} \cdot vds = - vdp \tag{B.3}$$

During the pure expansion process, the work done on the gas is

$$dW_2 = -pdv \tag{B.4}$$

where dv is the change in the volume v from v to v'. The kinetic energy per unit mass of the gas is

$$K = \frac{1}{2} u^2 \tag{B.5}$$

where u is the speed of mass flow at a location along the flow in the tube. Equating the differential work done on the gas and energy gained by the gas produces

$$- vdp - pdv = dE + udu \tag{B.6}$$

The differential of the enthalpy, h is defined as (28, p. 9)

$$dh = vdp + pdv + dE = C_p dT \tag{B.7}$$

where C_p is the specific heat at constant pressure. Integration of the energy equation with substitution of $C_p dT$ for the differential of the enthalpy produces the final energy equation for the gas:

$$\frac{1}{2} u^2 + C_p T = \text{Constant} \tag{B.8}$$

This energy equation describes how the effective temperature of the gas and the kinetic energy of mass flow are related: during the expansion process the temperature that could be observed by someone moving with the gas decreases as the flow velocity increases. Some of the energy of the random motion of the molecules has been converted during the expansion and flow. The effective temperature which is important in the considerations of random motion presented in Chapters 1 and 2, and, therefore, the range of speeds of the target molecules, is reduced by this expansion. In this manner the "cooling" is carried out in order to allow recognition of the structure in the time-of-flight spectrum of the H(2S) atoms.